

# Ex<sup>2</sup>MCMC: Sampling through Exploration Exploitation

Evgeny Lagutin<sup>1,2,5</sup>Daniil Selikhanovych<sup>1,5</sup>Achille Thin<sup>4</sup>Sergey Samsonov<sup>2</sup>Alexey Naumov<sup>2</sup>Denis Belomestny<sup>2,3</sup>Maxim Panov<sup>1</sup>Eric Moulines<sup>2,4</sup><sup>1</sup> Skoltech<sup>2</sup> HSE University<sup>3</sup> Duisburg-Essen University<sup>4</sup> Ecole Polytechnique<sup>5</sup> Moscow Institute of Physics and Technology

## Abstract

We develop an Explore-Exploit Markov chain Monte Carlo algorithm (Ex<sup>2</sup>MCMC) that combines multiple global proposals and local moves. The proposed method is massively parallelizable and extremely computationally efficient. We prove  $V$ -uniform geometric ergodicity of Ex<sup>2</sup>MCMC under realistic conditions, and compute explicit bounds on the mixing rate showing the improvement brought by the multiple global moves. We show that Ex<sup>2</sup>MCMC allows fine-tuning of exploitation (local moves) and exploration (global moves) via a novel approach to proposing dependent global moves. Finally, we develop an adaptive scheme, FlEx<sup>2</sup>MCMC, that learns the distribution of global moves using normalizing flows. We illustrate the efficiency of Ex<sup>2</sup>MCMC and its adaptive versions on many classical sampling benchmarks. We also show that these algorithms improve the quality of sampling GANs as energy-based models.

## 1 Introduction

Suppose one is interested in sampling from a probability distribution  $\Pi$  that is known up to a scaling factor. A Markov chain Monte Carlo algorithm (MCMC) consists of simulating a realization of a time-homogeneous Markov chain  $\{Y_k, k \in \mathbb{N}\}$  with the Markov kernel  $K$ , with the property that the distribution of  $Y_n$  becomes arbitrarily close to  $\Pi$  as  $n \rightarrow \infty$ , irrespective of the

distribution of  $Y_0$ . A property that the kernel  $K$  must satisfy is that it leaves the distribution  $\Pi$  invariant, i.e.,  $\Pi$  should be a fixed point of the Markov kernel. Instead, one can consider the stronger *detailed balance* condition or reversibility, a property that is easier to handle due to its local character. In particular, it leads to the famous Metropolis-Hastings (MH) kernel, the cornerstone of MCMC simulations, and a number of its successful variants.

To improve the available samplers, a number of authors have tried to optimize the usual MH algorithm by generating a pool of proposals at each iteration, e.g. Multiple-Try Metropolis algorithm (MTM; Liu et al. (2000); Craiu and Lemieux (2007)). The use of multiple proposals at each iteration, which can be efficiently implemented in parallel computing architectures, allows to increase the local search region without decreasing the acceptance ratio, which leads to an improvement in the mixing rate. This property has been theoretically supported by results on the high-dimensional scaling limit (see (Bédard et al., 2012)). At the same time, MCMC algorithms based on multiple independent proposals suffer from the fact that their acceptance rate decreases dramatically in large dimension. In this work, we follow the idea of generating multiple proposals for MH-based MCMC but give a new prospective on it and provide a computationally attractive alternative to MTM.

**Contributions** The main contributions of the paper are as follows:

- We propose an Explore-Exploit MCMC algorithm (Ex<sup>2</sup>MCMC), that retains most of the desirable properties of MTM, in particular, high degree of parallelization and improved mixing rate, while reducing the computational cost. We prove  $V$ -uniform geometric convergence of Ex<sup>2</sup>MCMC and evaluate its mixing rate;
- We propose an original method to construct dependent proposals for Ex<sup>2</sup>MCMC, which allows

to fine-tune the exploration-exploitation trade-off. Moreover, we propose an adaptive algorithm to learn the proposal distribution (FLEX<sup>2</sup>MCMC);

- We provide numerical evaluation of Ex<sup>2</sup>MCMC and FLEX<sup>2</sup>MCMC on various sampling problems, including sampling from GANs as energy-based model. The results clearly show the benefits of the proposed approaches compared to standard MCMC methods.

## 2 Ex<sup>2</sup>MCMC

### 2.1 From Importance Sampling to Sampling Importance Resampling

Importance Sampling (IS) is widely used for estimating integrals of the function  $f$  w.r.t. of a target distribution  $\Pi$  on a state-space  $(\mathbb{X}, \mathcal{X})$ , known up to a normalizing factor  $Z_\Pi$ ,  $\Pi(dx) = \tilde{\Pi}(dx)/Z_\Pi$ ; see, e.g. (Robert and Casella, 2013). IS consists of weighting samples from a proposal  $\Lambda$ . Assume that  $\tilde{\Pi}(dx) = \tilde{w}(x)\Lambda(dx)$ , and that the importance weight function  $\tilde{w}$  is positive, i.e.  $\tilde{w}(x) > 0$  for all  $x \in \mathbb{X}$ . We often assume that  $\tilde{\Pi}$  (hence,  $\Pi$ ) and  $\Lambda$  have positive densities w.r.t. a common dominating measure, denoted by  $\tilde{\pi}$ ,  $\pi$ , and  $\lambda$ , respectively. If this is the case,  $\tilde{w}(x) = \tilde{\pi}(x)/\lambda(x)$ . The *self-normalized importance sampling* (SNIS) estimator of  $\pi(f)$  is then given by  $\hat{\Pi}_N(f) = \sum_{i=1}^N \omega_N^i f(X^i)$ , where  $X^{1:N} \sim \Lambda$  and  $\omega_N^i = \tilde{w}(X^i)/\sum_{j=1}^N \tilde{w}(X^j)$ ,  $i \in \{1, \dots, N\}$  are the self-normalized importance weights.

Provided that  $\Lambda(\tilde{w}^2) = \int \tilde{w}(x)^2 \Lambda(dx) < \infty$ , the bias and the mean square error MSE of the SNIS estimator are inversely proportional to  $N$ .

Although importance sampling is primarily intended to approximate integrals of the form  $\Pi(f)$ , it can also be used to (approximately) sample from  $\Pi$ . The latter can be achieved by the Sampling Importance Resampling (SIR; Rubin (1987)). SIR is a two-stage procedure. In the first stage, an i.i.d. sample  $X^{1:N} = X^1, \dots, X^N$  is sampled from  $\Lambda$  and the importance weights  $\omega^{1:N} = \omega_N^1, \dots, \omega_N^N$  are computed. In a second step, a sample of size  $M$ ,  $Y^{1:M}$  is obtained by sampling with replacement with the weights  $\omega^{1:N}$ , denoted  $\text{Cat}(\omega^{1:N})$ . In other words, given a  $N$ -iid sample  $X^{1:N}$  from  $\Lambda$ , SIR draws samples from the empirical distribution  $\hat{\Pi}(dx) = \sum_{i=1}^N \omega_N^i \delta_{X^i}(dx)$  where  $\delta_y(dx)$  denotes the Dirac mass at  $y$ . As  $N \rightarrow \infty$ , a sample  $Y^1, \dots, Y^M \sim \hat{\Pi}$  will be distributed according to  $\Pi$ ; see (Smith and Gelfand, 1992; Skare et al., 2003). The main issue of SIR method is that it is only asymptotically valid.

### 2.2 From SIR to iterated Sampling Importance Resampling (i-SIR)

A closely related algorithm is the *iterated SIR* (i-SIR), a term coined in (Andrieu et al., 2010) and later

investigated more deeply in (Andrieu et al., 2018). For i-SIR, the sample size  $N$  is not necessarily large, but the process of sampling from the proposal, computing the normalized importance weights and picking a candidate is iterated. The  $j$ -th i-SIR iteration is defined as follows. Given the current state  $Y_j \in \mathbb{X}$ , (i) Set  $X_{j+1}^1 = Y_j$  and draw  $X_{j+1}^{2:N}$  independently from the proposal distribution  $\Lambda$ . (ii) Compute the normalized importance weights  $\omega_{N,j+1}^i = \tilde{w}(X_{j+1}^i)/\sum_{\ell=1}^N \tilde{w}(X_{j+1}^\ell)$ ,  $i \in \{1, \dots, N\}$ . (iii) Draw  $Y_{j+1}$  from the proposal set  $X_{j+1}^{1:N}$ , choosing  $X_{j+1}^i$  with probability  $\omega_{N,j+1}^i$ . The Markov kernel associated with i-SIR is given, for  $(x, A) \in \mathbb{X} \times \mathcal{X}$ , by

$$P_N(x, A) = \int \delta_x(dx^1) \sum_{i=1}^N \frac{\tilde{w}(x^i)}{\sum_{j=1}^N \tilde{w}(x^j)} 1_A(x^i) \prod_{j=2}^N \Lambda(dx^j). \quad (1)$$

**Lemma 1.**  $P_N$  admits  $\Pi$  as its invariant distribution.

This result is proven in (Andrieu et al., 2018) (see also Appendix B.1). To go further, we now establish the  $V$ -geometric convergence for i-SIR samples to  $\Pi$ . To state the results, we introduce, for a function  $V(x) : \mathbb{X} \mapsto [1, \infty)$ , the  $V$ -norm of two probability measures  $\xi$  and  $\xi'$  on  $(\mathbb{X}, \mathcal{X})$ ,  $\|\xi - \xi'\|_V := \sup_{|f(x)| \leq V(x)} |\xi(f) - \xi'(f)|$ . If  $V \equiv 1$ ,  $\|\cdot\|_1$  corresponds to the total variation distance (rather denoted  $\|\cdot\|_{TV}$ ).

**Definition 2** (Geometric Ergodicity). *A Markov kernel  $Q$  with invariant probability measure  $\Pi$  is  $V$ -geometrically ergodic if there exist constants  $\rho \in (0, 1)$  and  $M < \infty$  such that, for all  $k \in \mathbb{N}$ ,*

$$\|Q^k(x, \cdot) - \Pi\|_V \leq M V(x) \rho^k \quad \text{for all } x \in \mathbb{X}. \quad (2)$$

In particular, geometric ergodicity results ensure that the distribution of the  $n$ -th step of a Markov chain converges geometrically fast to the invariant probability in  $V$ -norm, for all starting points  $x \in \mathbb{X}$ . Here the dependence on the initial state  $x$  appears on the right-hand side only in  $V(x)$ . Uniform geometric ergodicity of i-SIR is established in (Andrieu et al., 2018, Theorem 1) under the assumption that the normalized importance weight function  $w$  (that is,  $\Pi(dx) = w(x)\Lambda(dx)$ ) is uniformly bounded.

This result is extended below for arbitrary  $V$ -norm satisfying  $\Pi(V) = \int V(x)\Pi(dx) < \infty$  under the following condition.

**A1.** For any  $x \in \mathbb{X}$ ,  $w(x) \leq L$ , with  $L < \infty$ .

The result is up to our best knowledge new.

**Theorem 3.** Assume **A 1**. Set  $\epsilon_N = \frac{N-1}{2L+N-2}$  and  $\kappa_N = 1 - \epsilon_N$ . Then,

(i) For any  $x \in \mathbb{X}$  and  $k \in \mathbb{N}$ ,  $\|P_N^k(x, \cdot) - \Pi\|_{TV} \leq \kappa_N^k$

**Algorithm 1:** Single stage of Ex<sup>2</sup>MCMC algorithm with independent proposals

---

**1 Procedure** Ex<sup>2</sup>MCMC ( $Y_j, \Lambda, R$ ):  
**Input** : Previous sample  $Y_j$ ;  
proposal distribution  $\Lambda$ ;  
rejuvenation kernel  $R$ ;  
**Output**: New sample  $Y_{j+1}$ ;  
Set  $X_{j+1}^1 = Y_j$ , draw  $X_{j+1}^{2:N} \sim \Lambda$ ;  
**for**  $i \in [N]$  **do**  
  compute the normalized weights  
   $\omega_{i,j+1} = \tilde{w}(X_{j+1}^i) / \sum_{k=1}^N \tilde{w}(X_{j+1}^k)$ ;  
Set  $I_{j+1} = \text{Cat}(\omega_{1,j+1}, \dots, \omega_{N,j+1})$ ;  
Draw  $Y_{j+1} \sim R(X_{j+1}^{I_{j+1}}, \cdot)$ .

---

Let  $V: \mathbb{X} \rightarrow [1, \infty)$  be any measurable function such that  $\Pi(V) < \infty$  and  $\Lambda(V) < \infty$ . Then,

(ii) For all  $x \in \mathbb{X}$  and  $k \in \mathbb{N}$ ,  $\|\mathbb{P}_N^k(x, \cdot) - \Pi\|_V \leq c_N \{\Pi(V) + V(x)\} \tilde{\kappa}_N^k$ , where the constants  $c_N, \tilde{\kappa}_N$  are given in (53).

The proof is postponed to Appendix B.2. We show that  $\tilde{\kappa}_N = O(N^{-1/3})$  which can be sharpen but essentially means that the geometric convergence rate decreases to 0 with the reciprocal of the number of proposals  $N$ . **A1** is restrictive, and even if it is satisfied, in most cases the upper bound grows exponentially with dimension (typically, if  $\Pi_d = \prod_{i=1}^d \Pi, \Lambda_d = \prod_{i=1}^d \Lambda$ , then  $L_d = L^d$ ). For this reason, IS is rarely used in high-dimensional space unless the proposal distribution is learned (Agapiou et al., 2017), which is the key point of Adaptive IS methods; see Section 3. A natural idea is to couple the i-SIR method with some local MCMC steps to define a sampler that remains  $V$ -uniformly geometrically ergodic even if **A1** is not satisfied. After each step of i-SIR, it suffices to apply a local MCMC kernel  $R$  (called *rejuvenation kernel*) that has  $\Pi$  as invariant distribution. We call this algorithm the Ex<sup>2</sup>MCMC algorithm because it combines steps of exploration by i-SIR and steps of exploitation by the local MCMC moves. The resulting Ex<sup>2</sup>MCMC algorithm is given by Algorithm 5.

We denote by  $K_N$  the associated Markov kernel (see Supplementary Material). Consider the following assumption

**A 2.** (i)  $R$  has  $\Pi$  as its unique invariant distribution; (ii) There exists a function  $V: \mathbb{X} \rightarrow [1, \infty)$ , such that for all  $d \geq d_R > 1$  there exist  $\lambda_{R,d} \in [0, 1)$ ,  $b_{R,d} < \infty$ , such that  $RV \leq \lambda_{R,d}V + b_{R,d}V_d$ , where  $V_d = \{x: V(x) \leq d\}$ ; (iii) For all  $d \geq d_R$ ,  $\sup_{x \in V_d} w(x) < w_{\infty,d} < \infty$ .

(ii) states that the rejuvenation kernel satisfies a Foster-Lyapunov drift condition for  $V$ : it is satisfied

by very many MCMC kernels, typically under super-exponential tail conditions for the target distribution; see (Roberts and Rosenthal, 2004) and (Douc et al., 2018, Chapter 2) and the references therein. (iii) states that the importance weights are upper bounded on level sets. This is a mild condition: if  $\mathbb{X} = \mathbb{R}^d$ , and  $V$  is norm-like, then the level sets  $V_d$  are compact and  $\tilde{w}$  is bounded as soon as  $\pi$  and  $\lambda$  are positive and continuous. We emphasize that we do not need to identify the small sets of the rejuvenation kernel. We can now present the main theoretical result of this paper.

**Theorem 4.** *Assume **A 2**. Then, for all  $x \in \mathbb{X}$  and  $k \in \mathbb{N}$ ,*

$$\|K_N^k(x, \cdot) - \Pi\|_V \leq c_{N,R}\{\Pi(V) + V(x)\} \tilde{\kappa}_{N,R}^k, \quad (3)$$

where the constant  $c_{N,R}, \tilde{\kappa}_{N,R}$  are given in (74).

The proof is postponed to Appendix B.3. The main steps are (i) establishing that the level sets  $V_d$  are small for the Markov kernel  $K_N$  (with a constant which depends only on  $N$  and  $w_{\infty,d}$ ; see Lemma 7); (ii) checking that  $K_N$  also satisfies a Foster-Lyapunov with function  $V$  with constant depending only on  $\lambda_{R,d} \in [0, 1)$ ,  $b_{R,d}$ , and  $N$ ; see Lemma 9. Note that  $\tilde{\kappa}_{N,R}$  typically decreases when the number of proposals  $N$  grows. In many situations, the mixing rate  $\tilde{\kappa}_{N,R}$  is significantly better than the corresponding mixing rate of  $R$ , provided that  $N$  is large enough. This is illustrated in Appendix C with the Metropolis Adjusted Langevin Algorithm (MALA) kernel (see e.g. (Besag, 1994; Roberts and Tweedie, 1996)).

### 2.3 Dependent proposals for i-SIR and Ex<sup>2</sup>MCMC algorithms

We now extend Ex<sup>2</sup>MCMC by relaxing the assumptions that the proposals at each stage are independent. The possibility of using dependent particles (and in particular *local moves* around the conditioning point) allows Ex<sup>2</sup>MCMC algorithm to fine-tune Exploration v.s. Exploitation. Denote by  $\bar{\Lambda}_N(dx^{1:N})$  the joint distributions of the proposed particles. The key property to satisfy is that the marginal distribution of the proposed particles is  $\Lambda$ , that is for each  $i \in [N] = \{1, \dots, N\}$  there exists a Markov kernel denoted  $Q_i$  satisfying

$$\Lambda(dx^i)Q_i(x^i, dx^{1:N \setminus \{i\}}) = \bar{\Lambda}_N(dx^{1:N}). \quad (4)$$

The Markov kernel  $Q_i(X^i, \cdot)$  defines the conditional distribution of the particles  $X^{1:N \setminus \{i\}}$  given the “conditioning” particle  $X^i$ . In the simple i-SIR case,  $Q_i(x^i, dx^{1:N \setminus \{i\}}) = \prod_{j \neq i} \Lambda(dx^j)$  so that  $\bar{\Lambda}_N(dx^{1:N}) = \prod_{i=1}^N \Lambda(dx^i)$ . Using these conditional distributions, we now adapt Algorithm 5 by changing line 1 by

1. Draw  $U_{j+1}$  from the uniform distribution in  $[N]$  and set  $X_{j+1}^{U_{j+1}} = Y_j$ ;

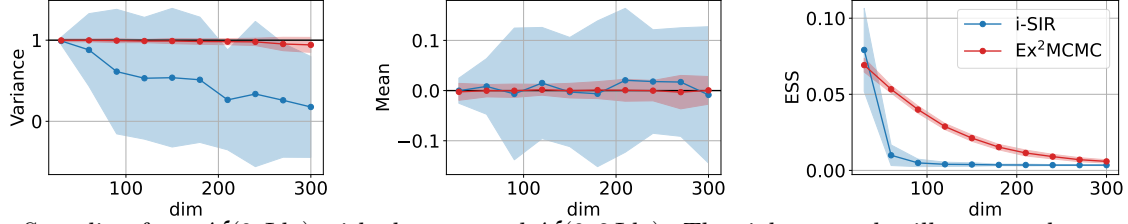


Figure 1: Sampling from  $\mathcal{N}(0, \text{Id}_d)$  with the proposal  $\mathcal{N}(0, 2 \text{Id}_d)$ . The rightmost plot illustrates the number of rejections rapidly growing for vanilla i-SIR algorithm (see Appendix F.1 for the definition of ESS). The correlated proposals in Ex<sup>2</sup>MCMC help to achieve efficient sampling even in high dimensions. We display confidence intervals for i-SIR and Ex<sup>2</sup>MCMC obtained from 20 independent runs as blue and red regions, respectively.

2. Draw  $X_{j+1}^{1:N \setminus \{U_{j+1}\}} \sim Q_{U_{j+1}}(X_{j+1}^{U_{j+1}}, \cdot)$ .

Note that *contrary to the independent case* we *randomize* the index of the conditioning variable, because we have not assumed that the joint proposal  $\bar{\Lambda}_N$  is exchangeable. We present below some methods of constructing proposals verifying (4). We denote by  $C_N$  the corresponding Markov kernel. The following result establishes the validity of the proposed algorithm, which holds virtually without any assumption.

**Theorem 5.** *For any  $N \geq 2$ , the Markov kernel  $C_N$  admits  $\Pi$  as its unique invariant distribution.*

We now describe a general method for constructing joint proposals  $\bar{\Lambda}_N$  with the proper marginal  $\Lambda$ . The main motivation for this construction is to seize the opportunity of massive parallelization of proposal sampling, which is a key to efficient implementation. The basic idea is to introduce a hierarchical latent variable model that allows flexible control of the dependency between proposals while preserving the desired symmetry property. Denote by  $(\mathbb{E}, \mathcal{E})$  the latent space,  $\Xi$  the latent distribution and  $R$ , a Markov kernel on  $\mathbb{E} \times \mathcal{X}$ , the conditional distribution of the proposal given the latent variable. We assume that

$$\mathbb{E}R(dx) = \int_{\mathbb{E}} \Xi(d\xi)R(\xi, dx) = \Lambda(dx). \quad (5)$$

We associate to each proposal  $X^i$  a latent variable  $\xi^i$ ,  $i \in [N]$ ;  $R(\xi^i, \cdot)$  therefore defines the conditional distribution of  $X^i$  given the latent variable  $\xi^i$ . Denote by  $\bar{\Xi}_N$  the joint distribution of  $\xi^{1:N}$ . It is assumed that the marginal distribution of any  $\xi^i$  is  $\Xi$ , and we denote by  $S_i$  the Markov kernel satisfying for any  $i \in [N]$ ,

$$\bar{\Xi}_N(d\xi^{1:N}) = \Xi(d\xi^i) S_i(\xi^i, d\xi^{1:N \setminus \{i\}}). \quad (6)$$

Finally, we set

$$\bar{\Lambda}_N(dx^{1:N}) = \int_{\mathbb{E}^N} \bar{\Xi}_N(d\xi^{1:N}) \prod_{i=1}^N R(\xi^i, dx^i). \quad (7)$$

This is the distribution of  $N$  random variables  $X^{1:N}$  taking values in  $\mathbb{X}$ . The variables  $\{X^i\}_{i=1}^N$  are conditionally independent with respect to the latent variables  $\xi^{1:N}$  and are marginally distributed according to

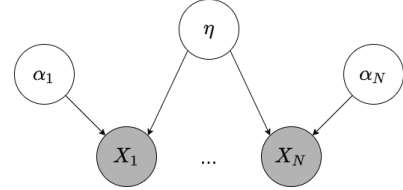


Figure 2: Graphical model for the proposals  $X^{1:N}$ .

$\Lambda$  thanks to (5). This helps to show that the distribution defined by (7) satisfies (4) with the properly selected kernel  $Q_i(x^i, dx^{1:N \setminus \{i\}})$ . Define by  $\check{R}$  the *reverse* Markov kernel on  $\mathbb{X} \times \mathcal{E}$  satisfying

$$\Xi(d\xi)R(\xi, dx) = \Lambda(dx)\check{R}(x, d\xi). \quad (8)$$

The Markov kernel  $\check{R}$  can be computed using the Bayes rule. This is transparent when the Markov kernel  $R$  has density, *i.e.* there exists a function  $r$  and a measure  $\mu$  on  $\mathbb{X}$  such that  $R(\xi, dx) = r(x | \xi)\mu(dx)$ . In this case  $r$  is the conditional p.d.f. of the proposal  $X$  given the latent variable  $\xi$ . In such case,  $\Lambda(dx) = \lambda(x)\mu(dx)$ , with  $\lambda(x) = \int_{\mathbb{E}} \Xi(d\xi)r(x | \xi)$  which is the marginal p.d.f. of the proposal  $X$ . The reversal condition in this case writes:  $\Xi(d\xi)R(\xi, dx) = r(x | \xi)\Xi(d\xi)\mu(dx) = r(x | \xi)/\lambda(x)\Xi(d\xi)\Lambda(dx)$ . This shows that the reverse kernel has a density w.r.t.  $\Xi$  given by  $\check{r}(\xi | x) = r(x | \xi)/\lambda(x)$ . Using (8), it is easily seen that for all  $i \in [N]$

$$\begin{aligned} Q_i(x^i, dx^{1:N \setminus \{i\}}) &= \\ &= \int_{\mathbb{E}^N} \check{R}(x^i, d\xi^i) S_i(\xi^i, d\xi^{1:N \setminus \{i\}}) \prod_{j \neq i} R(\xi^j, dx^j). \end{aligned} \quad (9)$$

We can then simply update Algorithm 5 by replacing line 1 by the following three steps:

1. Draw  $U_{j+1}$  from the uniform distribution in  $[N]$  and set  $X_{j+1}^{U_{j+1}} = Y_j$ ,  $\xi_{j+1}^{U_{j+1}} \sim \check{R}(X_{j+1}^{U_{j+1}}, \cdot)$ ,
2. Draw latents  $\xi_{j+1}^{1:N \setminus \{U_{j+1}\}} \sim S_{U_{j+1}}(\xi_{j+1}^{U_{j+1}}, \cdot)$ ,
3. Draw proposals  $X_{j+1}^i \sim R(\xi_{j+1}^i, \cdot)$ ,  $i \in [N] \setminus \{U_{j+1}\}$ .

Below we provide an example of Ex<sup>2</sup>MCMC algorithm with dependent proposal distributions.

---

**Algorithm 2:** Ex<sup>2</sup>MCMC for Gaussian proposal

---

**Input** : Sample  $Y_j$  from previous iteration  
**Output:** Set of proposals for the current iteration  $X_{j+1}^{1:N}$

- 1 Draw  $U_{j+1} \sim \text{Unif}([N])$  and set  $X_{j+1}^{U_{j+1}} = Y_j$
- 2 Draw  $\alpha_{j+1}^{U_{j+1}} \sim \nu$  and  $\eta_{j+1} \sim N(\alpha_{j+1}^{U_{j+1}} X_{j+1}^{U_{j+1}}, \sigma^2[\alpha_{j+1}^{U_{j+1}}] \text{Id}_d)$
- 3 For  $i \in [N] \setminus \{U_{j+1}\}$ , draw  $W_{j+1}^i \sim N(0, \text{Id}_d)$ ,  $\alpha_{j+1}^i \sim \nu$ , and set  $X_{j+1}^i = \alpha_{j+1}^i \eta_{j+1} + \sigma[\alpha_{j+1}^i] W_{j+1}^i$ .

---

## 2.4 Dependent Gaussian proposals

Let us denote by  $g(x; \mu, \Gamma)$  the Gaussian p.d.f. with mean  $\mu \in \mathbb{R}^d$  and covariance  $\Gamma \in \mathbb{R}^{d \times d}$ . Assume that the proposal distribution is Gaussian, *i.e.*  $\lambda(x) = g(x; 0, \sigma_\Lambda^2 \text{Id}_d)$ . As we will see below, this example is important because it is often used when sampling generative models. We give a step-by-step construction that closely follows the presentation given above. We first define the latent space  $\mathbb{E} = \mathbb{R}^d \times \mathbb{R}$ , the latent variable  $\xi = (\eta, \alpha)$ . We assume that the latent distribution is a product  $\Xi = \Lambda \otimes \nu$ , with  $\nu(d\alpha) = \epsilon \delta_a(d\alpha) + (1 - \epsilon) \delta_0(d\alpha)$ , with  $\epsilon \in [0, 1]$  and  $a \in [0, 1]$ . Expressed with random variables,  $X = \alpha\eta + \sigma[\alpha]W$ ,  $\sigma[\alpha] = \sigma_\Lambda(1 - \alpha^2)^{1/2}$  where  $(\alpha, W)$  are two independent random variables,  $\alpha$  takes two values  $a$  and  $0$  with probability and  $\mathbb{P}(\alpha = a) = \epsilon$ ,  $W \sim N(0, \sigma_\Lambda^2 \text{Id}_d)$ . Under these assumptions, the conditional p.d.f of the proposal sample  $x$  given the latent variable  $(\eta, \alpha)$  is given by  $r(x \mid (\eta, \alpha)) = g(x; \alpha\eta, \sigma^2[\alpha] \text{Id}_d)$ . The reverse kernel  $\check{R}$  defined by (8) can be written as  $\check{R}(x, d(\alpha, \eta)) = \epsilon g(\eta; ax, \sigma^2[a] \text{Id}_d) \delta_a(d\alpha) d\eta + (1 - \epsilon) g(\eta; 0, \sigma_\Lambda^2 \text{Id}_d) \delta_0(d\alpha)$ . We now specify the joint law of the latent variables to be, for  $i \in [N]$ ,

$$S_i(\xi^i, d\xi^{1:N \setminus \{i\}}) = \prod_{j \neq i} \delta_{\eta^j}(d\eta^j) \nu(d\alpha^j), \quad (10)$$

that is, the latent variables  $\eta^i$ ,  $i \in [N]$  are all equal, whereas that the random variables  $\alpha^{1:N \setminus \{i\}}$  are conditionally independent with the same distributions  $\nu$ . The graphical model for the resulting latent variables approach for dependent proposals generation is given in Figure 2. Now we can specify the modification of Algorithm 5 in this case by substituting its `line 1` by Algorithm 6.

The value  $\epsilon$  controls the exploration-exploitation ratio of Ex<sup>2</sup>MCMC. When  $\epsilon = 0$  we recover the independent i-SIR, and for  $\epsilon = 1$  i-SIR is bound only to local proposals. In our experiments, we find in practice that a value  $\epsilon \in (0, 1)$  is relevant. To illustrate the need for introducing dependencies between propo-

sitions, consider the toy problem of sampling a high-dimensional Gaussian distribution:  $\pi(x) = g(x; 0, \text{Id}_d)$  and  $\lambda(x) = g(x; 0, 2 \text{Id}_d)$ . This is admittedly an artificial problem, but it provides a diagnosis of why i-SIR fails in high dimensions and why Ex<sup>2</sup>MCMC (here with  $\epsilon = 1$  and without rejuvenation steps at all) works well (see Figure 1). Details of the experiment can be found in Supplementary Material, Appendix F.4.

## 2.5 Related Work

i-SIR has been proposed by Andrieu et al. (2010) and further developed in (Andrieu et al., 2018); see also (Lee et al., 2010; Lee, 2011). Andrieu et al. (2018) highlights the links of i-SIR with particle Gibbs methods, the main difference being that the proposal distribution is defined on the “path space” used in sequential Monte Carlo methods; see also (Doucet et al., 2015). Using this analogy, the rejuvenation kernel plays a role similar to the backward sampling kernel in the particle Gibbs with Backward Sampling (PGBS; Lindsten and Schön (2013)). The idea of making the moves dependent of the conditioning particle has been suggested in the PGBS context by Shestopaloff and Neal (2018).

Ex<sup>2</sup>MCMC algorithm can also be seen as a collapsed version of the Gibbs sampler proposed in (Tjelmeland, 2004). The algorithm also has similarities with the Multiple Tries Metropolis (MTM) algorithm, but the Ex<sup>2</sup>MCMC is both computationally simpler and displays more favorable mixing properties. In the MTM algorithm,  $N$  i.i.d. trial proposals  $\{X_{j+1}^i\}_{i=1}^N$  are drawn from a kernel  $T(y, \cdot)$  in each iteration: this is similar to Ex<sup>2</sup>MCMC sampling step, except that we do not require  $Q_j(x^j, dx^{1:N \setminus \{j\}}) = \prod_{j=1}^N T(x^j, dx^j)$ . In a second step, a sample  $Y_{j+1}^*$  is selected with probability proportional to the weights (the exact expression of the importance weights differs from ours, but this does not change the complexity of the algorithm). In a third step (see (Liu et al., 2000, section 2)),  $N - 1$  i.i.d. proposals are drawn from the kernel  $T(Y_{j+1}^*, \cdot)$  and the move is assumed to be  $Y_{j+1} = Y_{j+1}^*$  with a *generalized M-H* ratio, see (Liu et al., 2000, eq. 3). This step is bypassed in Ex<sup>2</sup>MCMC, which reduces the computational complexity by a factor of 2.

## 3 Adaptive Ex<sup>2</sup>MCMC algorithm

As mentioned earlier, the success of IS methods lies in an appropriate choice of proposal distribution. A classical approach is to define families of proposal distributions  $\{\lambda_\theta\}$  parameterized by some parameters  $\theta$  chosen to match the target distribution  $\tilde{\pi}$ . Such families can be obtained using a sequence of invertible transformations called normalizing flow (Papamakarios et al., 2021). Let  $T: \mathbb{X} \rightarrow \mathbb{X}$  be a  $C^1$  diffeomorphism. We denote the push-forward of measure  $\Lambda$  under  $T$ , that is, the distribution of  $Y = T(X)$  with  $X \sim \lambda$ , by  $T\#\Lambda$ .

---

**Algorithm 3:** Single stage of FlEx<sup>2</sup>MCMC. Steps of Ex<sup>2</sup>MCMC are done in parallel with common values of proposal parameters  $\theta_j$ . Step 4 updates the parameters using the gradient estimate obtained from all the chains.

---

**Input** : weights  $\theta_j$ , batch  $Y_j[1 : K]$   
**Output:** new weights  $\theta_{j+1}$ , batch  $Y_{j+1}[1 : K]$

- 1 **for**  $k \in [K]$  **do**
- 2    $Y_{j+1}[k] = \text{Ex}^2\text{MCMC} (Y_j[k], T_{\theta_j} \# \Lambda, R)$
- 3   Draw  $\bar{Z}[1 : K] \sim \Lambda$ .
- 4   Update  $\theta_{j+1} = \theta_j - \gamma \widehat{\nabla \mathcal{L}}(Y_{j+1}, \bar{Z}, \theta_j)$ .

---

The corresponding push-forward density is given by  $\lambda_T(y) = \lambda(T^{-1}(y)) J_{T^{-1}}(y)$ , where  $J_T$  denotes the Jacobian determinant of  $T$ ; see (Rezende and Mohamed, 2015; Kobyzev et al., 2020; Papamakarios et al., 2021) and references therein. The parameterized family of diffeomorphisms  $\{T_\theta\}$  defines a family of distributions  $\{\lambda_{T_\theta}\}$ , denoted for conciseness  $\{\lambda_\theta\}$ . The parameter  $\theta$  is then chosen to minimize a discrepancy between the target  $\pi$  and  $\lambda_\theta$ . This discrepancy can be e.g. a forward or backward divergence KL or another  $f$ -divergence; see e.g. (Papamakarios et al., 2021). The forward KL objective and its gradient are given by

$$\mathcal{L}^f(\theta) = \int \log \frac{\pi(x)}{\lambda_\theta(x)} \pi(x) dx, \quad (11)$$

$$\nabla \mathcal{L}^f(\theta) = - \int \nabla \log \lambda_\theta(x) \pi(x) dx. \quad (12)$$

The backward KL divergence and its gradient are given by

$$\mathcal{L}^b(\theta) = \int \log \frac{\lambda(x)}{\pi(T_\theta(x)) J_{T_\theta}(x)} \lambda(x) dx, \quad (13)$$

$$\nabla \mathcal{L}^b(\theta) = - \int \nabla \log (\pi(T_\theta(x)) J_{T_\theta}(x)) \lambda(x) dx. \quad (14)$$

Note that  $\nabla \mathcal{L}^b(\theta)$  does not depend on the normalizing constant of  $\pi$ . Thus we can compute unbiased estimates of  $\mathcal{L}^f(\theta)$  and  $\mathcal{L}^b(\theta)$ , given a sample  $Y[k] \sim \pi$  and  $Z[k] \sim \lambda$  for  $k \in [K]$ , by

$$\widehat{\nabla \mathcal{L}^f}(Y[1 : K], \theta) = - \frac{1}{K} \sum_{k=1}^K \nabla \log \lambda_\theta(Y[k]), \quad (15)$$

$$\widehat{\nabla \mathcal{L}^b}(Z[1 : K], \theta) = - \frac{1}{K} \sum_{k=1}^K \nabla \log (\tilde{\pi}(T_\theta(Z[k])) J_{T_\theta}(Z[k])). \quad (16)$$

We adapt the proposal distribution using a weighted combination of the forward and backward KL:  $\widehat{\mathcal{L}}(Y, Z, \theta) = \alpha_j \widehat{\mathcal{L}}^f(Y, \theta) + \beta_j \widehat{\mathcal{L}}^b(Z, \theta)$ ; see (Gabrié et al., 2021). In our experiments we use the following scheme for weights:  $\alpha_j = \min(1, \frac{3j}{n})$ ,  $\beta_j = (1 - \alpha_j)$ , where  $n$  is the number of optimization steps.

We introduce in the following a novel adaptive MCMC scheme, FlEx<sup>2</sup>MCMC, which combines normalizing flows and Ex<sup>2</sup>MCMC; see (Andrieu and Thoms, 2008; Liang et al., 2011) for a background on adaptive MCMC. The importance weights for FlEx<sup>2</sup>MCMC become  $\tilde{w}_\theta(x) = \tilde{\pi}(x)/\lambda_\theta(x)$ . The dependence between proposals can be introduced by first correlating samples with kernels  $\{Q_i\}_{i=1}^N$  which satisfy (4), and passing them through the flow  $T_\theta$  afterwards in order to enhance the initial proposal distribution  $\lambda$ . The  $j$ -th step of the algorithm is given in Algorithm 7. We essentially perform  $K$  independent Ex<sup>2</sup>MCMC steps with the same values of flow parameters  $\theta$  and then update parameters based on the gradient estimate obtained from all the chains.

## 4 Experiments

In this section we illustrate the efficiency of Ex<sup>2</sup>MCMC and FlEx<sup>2</sup>MCMC compared to standard MCMC methods. In all our experiments we use the MALA rejuvenation kernel, but it is also possible to use other kernels, e.g. HMC (Neal, 2011) or NUTS (Hoffman et al., 2014). For FlEx<sup>2</sup>MCMC proposals we use the RealNVP (Dinh et al., 2017) normalizing flows trained with the Adam optimizer (Kingma and Ba, 2015). Additional details on the experimental setup, including hyperparameters can be found in Supplementary material, Appendix F and Table 6. We assess sampling performance using the empirical Sliced Total Variation distance (STV, Kolouri et al. (2019)), Effective Sample Size (ESS, Kish (1965)) and the empirical Euclidean Earth Mover’s distance (EMD, Monge (1781)). These metrics are defined in Supplementary Material, Appendix F.1. The code reproducing the experiments can be found at <https://github.com/stat-ml/ex2mcmc>.

### 4.1 Sampling experiments

**Distributions with complex geometry** We study the ability of Ex<sup>2</sup>MCMC to sample from the banana-shaped distributions and funnel distributions in high dimensions. Analytical expressions for target distributions and experimental details can be found in Appendix F.5. We use the HMC-based NUTS sampler (Hoffman et al., 2014) to generate reference samples and compute STV, ESS and EMD for samples obtained from single run of MALA, Ex<sup>2</sup>MCMC and FlEx<sup>2</sup>MCMC. The numerical results for asymmetric banana distribution are shown on Figure 3 and for funnel distribution on Figure 10. We clearly observe the benefits of Ex<sup>2</sup>MCMC over MALA in approximation quality (see also Figure 4), while FlEx<sup>2</sup>MCMC allows to dramatically improve sampling efficiency.

**Allen-Cahn equation** We use FlEx<sup>2</sup>MCMC to sample from the invariant distribution of the Allen-Cahn stochastic differential equation; see (Allen and

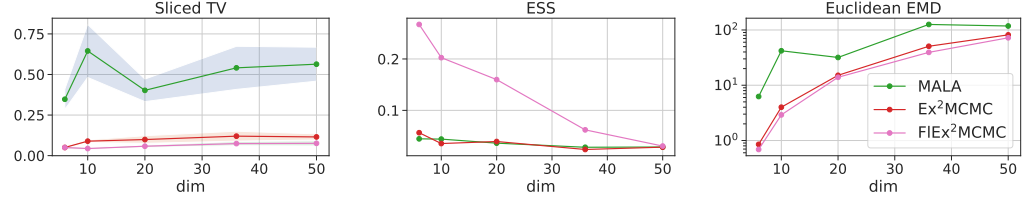
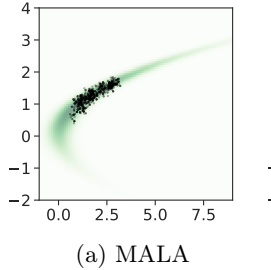
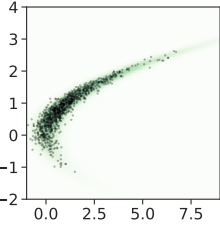


Figure 3: Sampling results for the asymmetric banana-shaped distribution. The Sliced TV, ESS and EMD metrics are reported as functions of the dimension of the space.



(a) MALA



(b) Ex<sup>2</sup>MCMC

Figure 4: Asymmetric banana-shaped distribution in dimension 50: projections on first two coordinates.

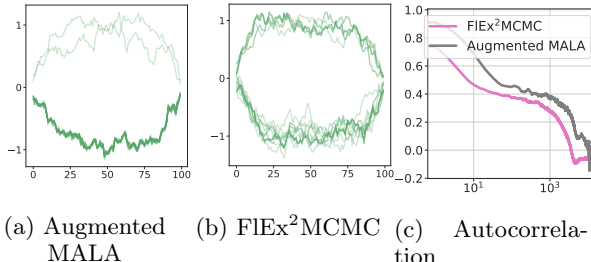


Figure 5: Allen-Cahn equation. Trajectories sampled by Augmented MALA and FlEx<sup>2</sup>MCMC and autocorrelation plot.

Cahn, 1975). For the details about distribution and task setting see (Gabrié et al., 2021) as we fully rely on it. In their paper they propose using normalizing flows to augment MALA algorithm that we further refer to as Augmented MALA. Figures 5a and 5b show examples of learned maps (100 examples per map) for MALA and FlEx<sup>2</sup>MCMC respectively. We observe that FlEx<sup>2</sup>MCMC is good in terms of exploring the sample space while MALA essentially sticks in few modes. Figure 5c shows the autocorrelations of the examples obtained during the burn-in period and training. We demonstrate that FlEx<sup>2</sup>MCMC allows for better mixing compared to method from (Gabrié et al., 2021). More details are provided in Supplementary Material, Appendix F.8.

**Bayesian Logistic Regression** Consider the training set  $\mathcal{D} = \{(x_j, y_j)\}_{j=1}^M$  consisting of pairs  $(x_j, y_j)$ , where  $x_j = (x_j^{(0)}, \dots, x_j^{(d-1)}) \in \mathbb{R}^d$  and labels  $y_j \in \{-1, 1\}$ . Without loss of generality, we assume that  $x_j^{(0)} = 1$ . The likelihood for a pair  $(x, y)$  is given by  $p(y | x, \theta) = \text{logit}(y \langle x, \theta \rangle)$ ,  $\theta \in \mathbb{R}^d$ . Given a prior distribution  $p_0(\theta)$ , we sample the posterior distribution  $p(\theta | \mathcal{D})$  and compute the posterior predictive

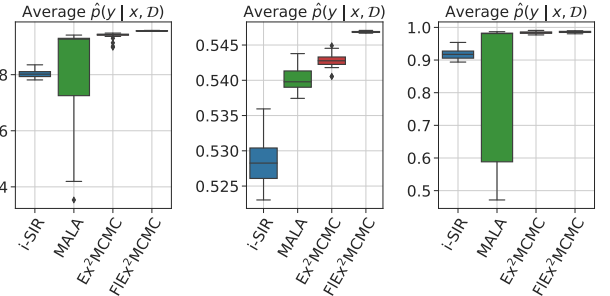


Figure 6: Bayesian logistic regression: average  $\hat{p}(y|x, \mathcal{D})$  for (left to right) Covertype, EEG and Digits datasets.

distribution  $p(y | x, \mathcal{D})$ . We approximate  $p(y | x, \mathcal{D})$  as  $p(y | x, \mathcal{D}) \simeq \frac{1}{n} \sum_{i=1}^n p(y | x, \mathcal{D}, \theta_i)$  for  $\theta_i \sim p(\cdot | \mathcal{D})$ ,  $i = 1, \dots, n$ . We display boxplots of the posterior predictive distribution averaged over the dataset based on 30 independent runs of the samplers, see Figure 6. The results show that Ex<sup>2</sup>MCMC achieves much higher values compared to i-SIR and MALA while FlEx<sup>2</sup>MCMC allows to further improve the average values and also simultaneously decrease the variance. The datasets and the implementation details are given in Supplementary Material, Appendix F.6.

#### 4.2 Sampling from GAN as Energy-based model (EBM)

Generative adversarial networks (GANs) represent a class of generative models defined by a pair of a generator network  $G$  and a discriminator network  $D$ . The generator  $G$  takes a latent variable  $z$  from a prior density  $p_0(z)$ ,  $z \in \mathbb{R}^d$ , and produces an observation  $G(z) \in \mathbb{R}^D$  in the observation space. The discriminator takes a sample in the observation space and aims to distinguish between real examples and fake ones, produced by the generator. Recently, it has been advocated that considering GAN as an energy-based model increases the quality of the generated samples (Turner et al., 2019; Che et al., 2020). Following Che et al. (2020), we consider the EBM model induced by the GAN on the latent space, contrary to (Turner et al., 2019) which works in the observation space. Recall that an EBM is defined by a Boltzmann-Gibbs distribution  $p(z) = e^{-E(z)}/Z$ ,  $z \in \mathbb{R}^d$ , where  $E(z)$  is the energy function and  $Z$  is the normalizing constant.

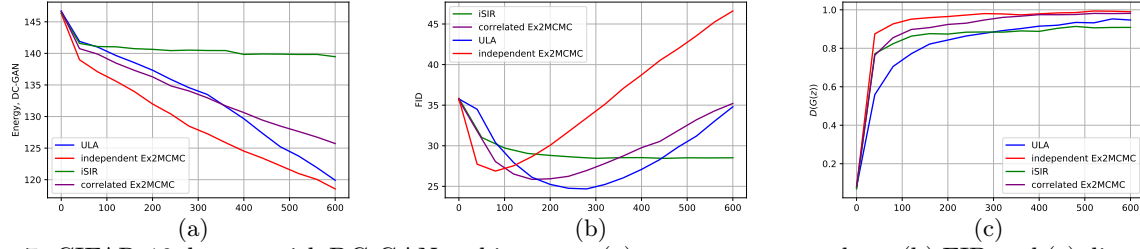


Figure 7: CIFAR-10 dataset with DC-GAN architecture: (a) average energy values, (b) FID and (c) discriminator scores for 600 sampling iterations.

We set  $E(z) = -\log p_0(z) - \text{logit}(D(G(z)))$ , where  $\text{logit}(y)$ ,  $y \in (0, 1)$  is the inverse of the sigmoid function and  $p_0(z) = g(z; 0; \text{Id}_d)$ . The distribution  $p(z)$  would perfectly reproduce the target one even for the imperfect generator, provided that the discriminator is optimal. In most EBMs, samples are generated from  $p(z)$  by an MCMC algorithm, either using the Unadjusted Langevin Dynamics (ULA) or standard MCMC algorithms like MALA or HMC; see (Xie et al., 2018; Nijkamp et al., 2020; Song and Kingma, 2021) and the references therein. We advocate using Ex<sup>2</sup>MCMC algorithm instead.

**GANs on synthetic data.** Following the setting used in (Che et al., 2020, Section 5.1), we apply Ex<sup>2</sup>MCMC to a WGAN model (Arjovsky et al., 2017) trained on synthetic datasets. Implementation details and additional experiments are provided in Supplement Material, Appendix F.11. Our first example is a mixture of  $M = 243$  Gaussians in  $\mathbb{R}^5$ , that is, the target distribution is  $M^{-1} \sum_{i=1}^M \mathcal{N}(\mu_i, \sigma^2 \text{Id}_5)$  with  $\sigma^2 = 1$  and centers  $\{\mu_i\}_{i=1}^M$  equally spaced on a uniform grid at  $\{-2; 0; 2\}^5$ . To assess the sampling performance, we first assign each point  $x$  to its closest mode  $\mu_{i(x)} = \arg \min_{j \in [M]} \|x - \mu_j\|^2$ . The point  $x$  is tagged as an *outlier* if  $\|x - \mu_{i(x)}\|^2 \geq t$ , where  $t$  is the 95% quantile of the  $\chi^2$ -distribution with 5 degrees of freedom. We compute *mode-std* as the sample variance of points in the neighborhood of each mode and number of captured modes as number of modes which were assigned with at least one point from the sample. We also compute the empirical Earth Mover’s distance (EMD) between the target and the empirical distribution. When applicable, we provide results both for single-start and multi-start regimes (see Appendix F.11 for more details). Results are summarized in Tables 1 and 2. This example illustrates that Langevin-based methods explore the support of distribution only in the multi-start regime. At the same time, each particular chain tends to stuck in one of the modes of the latent distribution  $p(z)$ . At the same time, Ex<sup>2</sup>MCMC allows to achieve high sampling quality even for the single chain.

**GANs for CIFAR-10.** In this experiment we investigate performance of Ex<sup>2</sup>MCMC algorithm for sam-

pling from EBM for GAN on the CIFAR10 dataset. As a GAN model we consider two popular architectures, DC-GAN (Radford et al., 2016) and SN-GAN (Miyato et al., 2018).

We compare ULA, i-SIR, and Ex<sup>2</sup>MCMC (both with correlated and independent proposals) methods. To evaluate sampling quality, we report the values of the energy function  $E(z)$ , averaged over 1000 independent runs of each sampler. We present the results on Figure 7 together with the dynamics of the Frechet Inception Distance (FID, Heusel et al. (2017)), computed over the first 600 sampler iterations. Additional implementation details are provided in Appendix A. Note that all methods except for i-SIR improve in terms of average energy function values, and Ex<sup>2</sup>MCMC algorithms allows for the best exploration.

At the same time, Figure 8b indicates that more accurate sampling from  $p(z)$  does not yield the desired FID improvement. Indeed, after 600 MCMC steps the best FID score corresponds to i-SIR procedure, which keeps energy function almost constant. Hence, essentially the issue is not with sampling from  $p(z)$ , but with calibrating the EBM for  $p(z)$  itself. An interesting future research direction is to check, if the discriminator training procedure or calibration could help to improve the model quality. The reported result is hard to compare with the ones in (Che et al., 2020), since the authors of it do not show the dynamics of FID score. We provide additional experiments (including the ones with SN-GAN) and visualizations in Appendix A.

Table 1: GAN sampling from 243 Gaussians

Model	mode std		# captured modes		EMD	
	Mult	Single	Mult	Single	Mult	Single
Vanilla GAN		0.040		34.8		3.86
ULA (Che et al., 2020)	0.039	0.022	98	1	4.20	30.96
MALA	0.040	0.030	85.8	3.5	3.80	24.03
Ex <sup>2</sup> MCMC	0.039	0.030	89.4	62.9	3.60	3.78

Table 2: Results for Swiss Roll dataset

Model	EMD		STV	
	Mult	Single	Mult	Single
WGAN-GP		0.011		0.053
ULA (Che et al., 2020)	0.010	2.961	0.048	0.91
MALA	0.010	0.055	0.051	0.056
Ex <sup>2</sup> MCMC	0.011	0.043	0.063	0.046

## 5 Conclusions

We propose a new MCMC algorithm, Ex<sup>2</sup>MCMC, which allows to improve over the competitors due to the efficiency both at exploration and exploitation steps. We analyze its theoretical properties and suggest an adaptive version of the algorithm, FlEx<sup>2</sup>MCMC, based on normalizing flows. It allows to overcome the issues of MTM and i-SIR algorithms, which are caused by low acceptance rate when sampling from high dimensional distributions. Further studies of FlEx<sup>2</sup>MCMC, in particular its mixing rate, is an interesting direction for the future work.

## References

Agapiou, S., Papaspiliopoulos, O., Sanz-Alonso, D., and Stuart, A. M. (2017). Importance sampling: Intrinsic dimension and computational cost. *Statistical Science*, 32(3):405–431.

Allen, S. M. and Cahn, J. W. (1975). Coherent and incoherent equilibria in iron-rich iron-aluminum alloys. *Acta Metallurgica*, 23(9):1017–1026.

Andrieu, C., Doucet, A., and Holenstein, R. (2010). Particle Markov chain Monte Carlo methods. *Journal of the Royal Statistical Society: Series B*, 72(3):269–342.

Andrieu, C., Lee, A., Vihola, M., et al. (2018). Uniform ergodicity of the iterated conditional SMC and geometric ergodicity of particle Gibbs samplers. *Bernoulli*, 24(2):842–872.

Andrieu, C. and Thoms, J. (2008). A tutorial on adaptive MCMC. *Statistics and computing*, 18(4):343–373.

Arjovsky, M., Chintala, S., and Bottou, L. (2017). Wasserstein generative adversarial networks. In *International conference on machine learning*, pages 214–223. PMLR.

Azadi, S., Olsson, C., Darrell, T., Goodfellow, I., and Odena, A. (2018). Discriminator Rejection Sampling. In *International Conference on Learning Representations*.

Azadi, S., Olsson, C., Darrell, T., Goodfellow, I., and Odena, A. (2019). Discriminator rejection sampling. *arXiv:1810.06758*.

Bédard, M., Douc, R., and Moulines, E. (2012). Scaling analysis of multiple-try MCMC methods. *Stochastic Processes and their Applications*, 122(3):758–786.

Besag, J. (1994). Comments on “Representations of knowledge in complex systems” by U. Grenander and M. Miller. *J. Roy. Statist. Soc. Ser. B*, 56:591–592.

Bonneel, N., Van De Panne, M., Paris, S., and Heidrich, W. (2011). Displacement interpolation using lagrangian mass transport. In *Proceedings of the 2011 SIGGRAPH Asia Conference*, pages 1–12.

Che, T., ZHANG, R., Sohl-Dickstein, J., Larochelle, H., Paull, L., Cao, Y., and Bengio, Y. (2020). Your GAN is Secretly an Energy-based Model and You Should Use Discriminator Driven Latent Sampling. In Larochelle, H., Ranzato, M., Hadsell, R., Balcan, M. F., and Lin, H., editors, *Advances in Neural Information Processing Systems*, volume 33, pages 12275–12287. Curran Associates, Inc.

Craiu, R. V. and Lemieux, C. (2007). Acceleration of the multiple-try Metropolis algorithm using anti-thetic and stratified sampling. *Statistics and Computing*, 17(2):109.

Dinh, L., Sohl-Dickstein, J., and Bengio, S. (2017). Density estimation using real NVP. In *5th International Conference on Learning Representations, ICLR 2017, Toulon, France, April 24-26, 2017, Conference Track Proceedings*.

Douc, R., Moulines, E., Priouret, P., and Soulier, P. (2018). *Markov chains*. Springer Series in Operations Research and Financial Engineering. Springer, Cham.

Doucet, A., Pitt, M. K., Deligiannidis, G., and Kohn, R. (2015). Efficient implementation of Markov chain Monte Carlo when using an unbiased likelihood estimator. *Biometrika*, 102(2):295–313.

Durmus, A., Moulines, E., and Saksman, E. (2017). On the convergence of Hamiltonian Monte Carlo. *arXiv preprint arXiv:1705.00166*.

Gabrié, M., Rotskoff, G. M., and Vanden-Eijnden, E. (2021). Adaptive Monte Carlo augmented with normalizing flows. *arXiv preprint arXiv:2105.12603*.

Goodfellow, I. J., Pouget-Abadie, J., Mirza, M., Xu, B., Warde-Farley, D., Ozair, S., Courville, A., and Bengio, Y. (2014). Generative adversarial nets. In *Proceedings of the 27th International Conference on Neural Information Processing Systems - Volume 2*, NIPS’14, page 2672–2680, Cambridge, MA, USA. MIT Press.

Haario, H., Saksman, E., and Tamminen, J. (1999). Adaptive proposal distribution for random walk metropolis algorithm. *Computational Statistics*, 14(3):375–395.

Heusel, M., Ramsauer, H., Unterthiner, T., Nessler, B., and Hochreiter, S. (2017). GANs Trained by a Two Time-Scale Update Rule Converge to a Local Nash Equilibrium. In Guyon, I., Luxburg, U. V., Bengio, S., Wallach, H., Fergus, R., Vishwanathan,

S., and Garnett, R., editors, *Advances in Neural Information Processing Systems*, volume 30. Curran Associates, Inc.

Hoffman, M. D., Gelman, A., et al. (2014). The no-U-turn sampler: adaptively setting path lengths in Hamiltonian Monte Carlo. *J. Mach. Learn. Res.*, 15(1):1593–1623.

Kingma, D. P. and Ba, J. (2015). Adam: A method for stochastic optimization. In *ICLR 2015*.

Kish, L. (1965). *Survey sampling*. Chichester : Wiley New York.

Kobyzev, I., Prince, S., and Brubaker, M. (2020). Normalizing flows: An introduction and review of current methods. *IEEE Transactions on Pattern Analysis and Machine Intelligence*.

Kolouri, S., Nadjahi, K., Simsekli, U., Badeau, R., and Gustavo, K. (2019). Generalized sliced Wasserstein distances. In *NeurIPS 2019*.

Laurent, B. and Massart, P. (2000). Adaptive estimation of a quadratic functional by model selection. *Ann. Statist.*, 28(5):1302–1338.

Lee, A. (2011). *On auxiliary variables and many-core architectures in computational statistics*. PhD thesis, University of Oxford.

Lee, A., Yau, C., Giles, M. B., Doucet, A., and Holmes, C. C. (2010). On the utility of graphics cards to perform massively parallel simulation of advanced Monte Carlo methods. *Journal of computational and graphical statistics*, 19(4):769–789.

Liang, F., Liu, C., and Carroll, R. (2011). *Advanced Markov chain Monte Carlo methods: learning from past samples*, volume 714. John Wiley & Sons.

Lindsten, F. and Schön, T. B. (2013). Backward simulation methods for Monte Carlo statistical inference. *Foundations and Trends® in Machine Learning*, 6(1):1–143.

Liu, J. S., Liang, F., and Wong, W. H. (2000). The multiple-try method and local optimization in Metropolis sampling. *Journal of the American Statistical Association*, 95(449):121–134.

Miyato, T., Kataoka, T., Koyama, M., and Yoshida, Y. (2018). Spectral normalization for generative adversarial networks. *arXiv:1802.05957*.

Monge, G. (1781). Mémoire sur la théorie des déblais et des remblais. *Histoire de l'Académie Royale des Sciences de Paris*.

Neal, R. M. (2011). MCMC using Hamiltonian dynamics. *Handbook of Markov Chain Monte Carlo*, pages 113–162.

Nijkamp, E., Hill, M., Han, T., Zhu, S.-C., and Wu, Y. N. (2020). On the anatomy of MCMC-based maximum likelihood learning of energy-based models. In *Proceedings of the AAAI Conference on Artificial Intelligence*, volume 34, pages 5272–5280.

Papamakarios, G., Nalisnick, E., Rezende, D. J., Mohamed, S., and Lakshminarayanan, B. (2021). Normalizing flows for probabilistic modeling and inference. *Journal of Machine Learning Research*, 22(57):1–64.

Radford, A., Metz, L., and Chintala, S. (2016). Unsupervised representation learning with deep convolutional generative adversarial networks. *arXiv:1511.06434*.

Rezende, D. and Mohamed, S. (2015). Variational inference with normalizing flows. In Bach, F. and Blei, D., editors, *Proceedings of the 32nd International Conference on Machine Learning*, volume 37 of *Proceedings of Machine Learning Research*, pages 1530–1538, Lille, France. PMLR.

Robert, C. and Casella, G. (2013). *Monte Carlo statistical methods*. Springer Science & Business Media.

Roberts, G. O. and Rosenthal, J. S. (2004). General state space Markov chains and MCMC algorithms. *Probability surveys*, 1:20–71.

Roberts, G. O. and Tweedie, R. L. (1996). Geometric convergence and central limit theorems for multidimensional Hastings and Metropolis algorithms. *Biometrika*, 83(1):95–110.

Rubin, D. B. (1987). Comment: A noniterative Sampling/Importance Resampling alternative to the data augmentation algorithm for creating a few imputations when fractions of missing information are modest: The SIR algorithm. *Journal of the American Statistical Association*, 82(398):542–543.

Shestopaloff, A. Y. and Neal, R. M. (2018). Sampling latent states for high-dimensional non-linear state space models with the embedded HMM method. *Bayesian Analysis*, 13(3):797–822.

Skare, Ø., Bølviken, E., and Holden, L. (2003). Improved sampling-importance resampling and reduced bias importance sampling. *Scandinavian Journal of Statistics*, 30(4):719–737.

Smith, A. F. and Gelfand, A. E. (1992). Bayesian statistics without tears: a sampling–resampling perspective. *The American Statistician*, 46(2):84–88.

Song, Y. and Kingma, D. P. (2021). How to train your energy-based models. *arXiv preprint arXiv:2101.03288*.

Tanaka, A. (2019). Discriminator optimal transport. In *Proceedings of the 33rd International Conference*

*on Neural Information Processing Systems*, pages 6816–6826.

Tjelmeland, H. (2004). Using all Metropolis–Hastings proposals to estimate mean values. Technical report.

Turner, R., Hung, J., Frank, E., Saatchi, Y., and Yosinski, J. (2019). Metropolis-Hastings generative adversarial networks. In *International Conference on Machine Learning*, pages 6345–6353. PMLR.

Wainwright, M. J. (2019). *High-Dimensional Statistics: A Non-Asymptotic Viewpoint*. Cambridge Series in Statistical and Probabilistic Mathematics. Cambridge University Press.

Xie, J., Lu, Y., Gao, R., and Wu, Y. N. (2018). Cooperative learning of energy-based model and latent variable model via MCMC teaching. In *Proceedings of the AAAI Conference on Artificial Intelligence*, volume 32.

## Supplementary Material

### A Sampling GANs as energy-based model on CIFAR-10

We consider two popular GAN architectures, DC-GAN Radford et al. (2016) and SN-GAN Miyato et al. (2018). Below we provide the details on experimental setup and evaluation for both of the models.

#### A.1 DC-GAN

For DC-GAN experiments, we took the pretrained GAN model after 200 epochs from the open repository <https://github.com/csinva/gan-vae-pretrained-pytorch>, to compute FID we took code from the repository <https://github.com/abdulfatir/gan-metrics-pytorch>.

For DC-GAN, the latent dimension equals  $d = 100$ . Following Che et al. (2020), we consider sampling from the latent space distribution

$$p(z) = e^{-E(z)}/Z, \quad z \in \mathbb{R}^d, \quad E(z) = -\log p_0(z) - \text{logit}(D(G(z))), \quad (17)$$

where  $\text{logit}(y) = \log(y/(1-y))$ ,  $y \in (0, 1)$  is the inverse of the sigmoid function, and  $p_0(z) = g(z; 0; \text{Id}_d)$ . For the step size  $\gamma > 0$  we define  $(k+1)$ -th iteration of the Unadjusted Langevin Algorithm as

$$Z_{k+1} = Z_k - \gamma \nabla E(Z_k) + \sqrt{2\gamma} \varepsilon_{k+1}, \quad \varepsilon_{k+1} \sim \mathcal{N}(0, \text{Id}_d). \quad (18)$$

Note that the ergodic distribution of the corresponding continuous-time diffusion is given by  $p(z) = e^{-E(z)}/Z$ . We specify our choice of  $\gamma$  in Table 6.

**Evaluation protocol** We run  $n = 600$  iterations of the ULA, i-SIR, and Ex<sup>2</sup>MCMC algorithm in its correlated and vanilla versions. For the vanilla Ex<sup>2</sup>MCMC algorithm (Algorithm 5), we use the Markov kernel (80), corresponding to 1 MALA step, as the rejuvenation kernel. Step size  $\gamma$ , reported for Ex<sup>2</sup>MCMC algorithm, corresponds to its rejuvenation MALA kernel. For the correlated Ex<sup>2</sup>MCMC algorithm (see Algorithm 6), we bypass the rejuvenation step, since local exploration is guaranteed by selecting large  $\alpha$ . Additional details are provided at Table 3.

We run  $N = 50000$  independent chains for each of the mentioned MCMC algorithms. Then, for  $j$ -th iteration, we calculate average value of the energy function  $E(z)$  averaged over  $M = 1000$  chains. Every 40 MCMC iterations we calculate FID based on 50000 images generated on the current MCMC step and 50000 images from the training data. We report FID results after 600 MCMC iterations at Table 5.

#### A.2 SN-GAN

For SN-GAN, we took an implementation available at [https://github.com/pfnet-research/sngan\\_projection](https://github.com/pfnet-research/sngan_projection) to reproduce results with the unconditional version of SN-GAN pretrained on CIFAR-10, to compute FID we took statistics from the repository <https://github.com/pfnet-research/chainer-gan-lib/blob/master/common/cifar-10-fid.npz>, used in the SN-GAN repository. We additionally calibrated SN-GAN discriminator as suggested at Azadi et al. (2019), by replacing its top linear layer with fully-connected one consisting of 3 consecutive linear layers and finetuning them with binary cross entropy loss for  $5k$  iterations.

Method	sampl. steps	$\gamma$	# particles, $N$	$\epsilon$	$\alpha$	num MALA steps
ULA	600	0.01	—	—	—	—
i-SIR	600	—	5	—	—	—
Vanilla Ex <sup>2</sup> MCMC	600	0.02	5	—	—	1
Correlated Ex <sup>2</sup> MCMC	600	—	5	0.9	0.99	0

Table 3: CIFAR-10 hyperparameters for DC-GAN architecture.

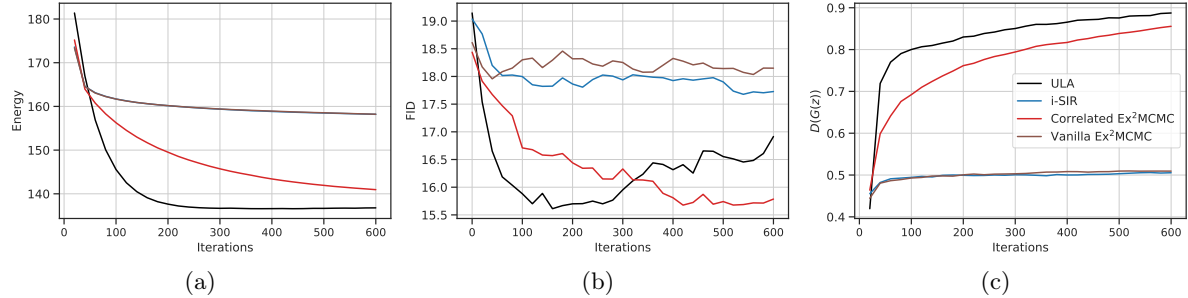


Figure 8: CIFAR-10 dataset with SN-GAN architecture: (a) average energy values, (b) FID and (c) discriminator scores for first 600 sampling iterations.

For SN-GAN, generator is a mapping  $G(z) : \mathbb{R}^d \mapsto \mathbb{R}^D$  with latent dimension  $d = 128$  and ambient space dimension  $D = 784$ . Following Che et al. (2020), we performed an additional tempering of the distribution, that is, we sampled from the energy-based model

$$p(z) = e^{-E(z)/T} / Z, \quad z \in \mathbb{R}^d, \quad E(z) = -\log p_0(z) - \text{logit}(D(G(z))). \quad (19)$$

In our experiments we observe, that simply setting  $T = 1$  does not yield significant sampling quality improvement, compared to vanilla GAN sampling. At the same time, setting  $T = 1/4$  allows to efficiently reduce the FID values, as reported in Figure 8.

Note that i-SIR and Ex2-MCMC with independent proposals fail to improve sampling quality compared to the vanilla GAN sampling, as it can be observed from Figure 8c-(a), and average discriminator scores  $D(G(z))$ , see Figure 8c-(c). Indeed, average discriminator score does not increase. At the same time, both ULA and Ex<sup>2</sup>MCMC with correlated particles shows considerable energy score improvement and better explore the regions of  $p(z)$  with large values  $D(G(z))$ . Ex<sup>2</sup>MCMC shows more stable behaviour in terms of FID metrics, reported in Figure 8c-(b).

The evaluation protocol for SN-GAN follows the one for DC-GAN but with some adjustments, see the value of hyperparameters in Table 4. We run  $N = 5000$  independent chains for each of the mentioned MCMC algorithms. Then, for  $j$ -th iteration, we calculate average value of the energy function  $E(z)$  averaged over  $N$  chains. Every 20 MCMC iterations we calculate FID based on 5000 images generated on the current MCMC step and 5000 images from the training data. We report FID results after 600 MCMC iterations at Table 5.

## B Proofs of main theoretical results of Section 2

**Notations** For  $k \in \mathbb{N}$ ,  $m, m' \in \mathbb{N}^*$  and  $\Omega, \Omega'$  two open sets of  $\mathbb{R}^m, \mathbb{R}^{m'}$  respectively, denote by  $C^k(\Omega, \Omega')$ , the set of  $k$ -times continuously differentiable functions. For  $f \in C^2(\mathbb{R}^d, \mathbb{R})$ , denote by  $\nabla f$  the gradient of  $f$  and by  $\Delta f$  the Laplacian of  $f$ . For  $k \in \mathbb{N}$  and  $f \in C^k(\mathbb{R}^d, \mathbb{R})$ , denote by  $D^i f$  the  $i$ -th order differential of  $f$  for  $i \in \{0, \dots, k\}$ . For  $x \in \mathbb{R}^d$  and  $i \in \{1, \dots, k\}$ , define  $\|D^0 f(x)\| = |f(x)|$ ,  $\|D^i f(x)\| = \sup_{u_1, \dots, u_i \in \mathbb{S}(\mathbb{R}^d)} D^i f(x)[u_1, \dots, u_i]$ . For  $k, p \in \mathbb{N}$  and  $f \in C^k(\mathbb{R}^d, \mathbb{R})$ , define

$$\|f\|_{k,p} = \sup_{x \in \mathbb{R}^d, i \in \{0, \dots, k\}} \|D^i f(x)\| / (1 + \|x\|^p). \quad (20)$$

Method	sampl. steps	$\gamma$	# particles, $N$	$\epsilon$	$\alpha$	num MALA steps
ULA	600	0.0025	—	—	—	—
i-SIR	600	—	4	—	—	—
Vanilla Ex <sup>2</sup> MCMC	600	0.005	4	—	—	1
Correlated Ex <sup>2</sup> MCMC	600	—	4	0.5	0.995	0

Table 4: CIFAR-10 hyperparameters for SN-GAN architecture.

Table 5: FID for CIFAR-10 GAN-based models

Model	SN-GAN	DC-GAN
Vanilla GAN	18.9	35.8
ULA (Che et al., 2020)	17.0	34.8
i-SIR	17.7	28.5
Correlated Ex <sup>2</sup> MCMC	15.8	35.2

Define  $C_{\text{poly}}^k(\mathbb{R}^d, \mathbb{R}) = \{f \in C^k(\mathbb{R}^d, \mathbb{R}) : \inf_{p \in \mathbb{N}} \|f\|_{k,p} < +\infty\}$  and for any  $f \in C_{\text{poly}}^k(\mathbb{R}^d, \mathbb{R})$ , we consider the semi-norm

$$\|f\|_k = \|f\|_{k,p} \text{ where } p = \min\{q \in \mathbb{N} : \|f\|_{k,q} < +\infty\}. \quad (21)$$

Finally, define  $C_{\text{poly}}^\infty(\mathbb{R}^d, \mathbb{R}) = \cap_{k \in \mathbb{N}} C_{\text{poly}}^k(\mathbb{R}^d, \mathbb{R})$ .

In the sequel, we denote by  $w(x)$  the normalized weight function, that is,

$$\Pi(dx) = w(x)\Lambda(dx). \quad (22)$$

### B.1 Proof of Lemma 1

By symmetrisation, note that

$$\mathsf{P}_N(x, \mathsf{A}) = \int \delta_x(dx_1) \sum_{i=1}^N \frac{w(x^i)}{\sum_{j=1}^N w(x^j)} \mathbf{1}_{\mathsf{A}}(x^i) \prod_{j=2}^N \Lambda(dx^j) \quad (23)$$

$$= \frac{1}{N} \int \sum_{\ell=1}^N \delta_x(dx_\ell) \prod_{j \neq \ell} \Lambda(dx^j) \sum_{i=1}^N \frac{w(x^i)}{\sum_{\ell=1}^N w(x^\ell)} \mathbf{1}_{\mathsf{A}}(x^i). \quad (24)$$

Then,

$$\int \Pi(dx) \mathsf{P}_N(x, \mathsf{A}) = N^{-1} \int \Pi(dx) \sum_{\ell=1}^N \delta_x(dx_\ell) \prod_{j \neq \ell} \Lambda(dx^j) \sum_{i=1}^N \frac{w(x^i)}{\sum_{\ell=1}^N w(x^\ell)} \mathbf{1}_{\mathsf{A}}(x^i) \quad (25)$$

$$= N^{-1} \int \left( \sum_{\ell=1}^N w(x_\ell) \right) \prod_{j=1}^N \Lambda(dx^j) \sum_{i=1}^N \frac{w(x^i)}{\sum_{\ell=1}^N w(x^\ell)} \mathbf{1}_{\mathsf{A}}(x^i) \quad (26)$$

$$= N^{-1} \int \prod_{j=1}^N \Lambda(dx^j) \sum_{i=1}^N w(x^i) \mathbf{1}_{\mathsf{A}}(x^i) = \Pi(\mathsf{A}) \quad (27)$$

### B.2 Proof of Theorem 3

We preface the proof by a technical lemma.

**Lemma 6.** *Let  $Y^{1:M}$  be i.i.d. random variables, such that  $\mathbb{E}[Y_1] = 1$ , and  $\mathbb{P}(Y_1 \in [0, L]) = 1$ . Then for  $S = \sum_{i=1}^M Y_i$  and  $a, b > 0$*

$$\mathbb{E} \left[ (a + bS)^{-1} \right] \leq (a + bM/2)^{-1} + (1/a) \exp(-M/(2L^2)). \quad (28)$$

*Proof.* Let  $K \geq 0$ . Then we get

$$\frac{1}{a + bS} = \frac{1}{a + bS} \mathbf{1}\{S < K\} + \frac{1}{a + bS} \mathbf{1}\{S \geq K\} \quad (29)$$

$$\leq \frac{1}{a + bK} \mathbf{1}\{S \geq K\} + \frac{1}{a + bS} \mathbf{1}\{S < K\} \leq \frac{1}{a + bK} + \frac{1}{a} \mathbf{1}\{S < K\} \quad (30)$$

and in particular,  $\mathbb{E}[(a + bS)^{-1}] \leq (a + bK)^{-1} + a^{-1} \mathbb{P}(S < K)$ . By Hoeffding's inequality,

$$\mathbb{P}(S < K) = \mathbb{P}(S - M < -(M - K)) \leq \exp(-2(M - K)^2/(ML^2)). \quad (31)$$

In particular, for  $K = M/2$ , we have  $\mathbb{P}(S < K) \leq \exp(-M/(2L^2))$ .  $\square$

*Proof of Theorem Theorem 3.* (i) Under **A1**, we have, for  $(x, \mathbf{A}) \in \mathbb{X} \times \mathcal{X}$ ,

$$\mathbf{P}_N(x, \mathbf{A}) = \int \delta_x(dx^1) \sum_{i=1}^N \frac{w(x^i)}{\sum_{j=1}^N w(x^j)} 1_{\mathbf{A}}(x^i) \prod_{j=2}^N \Lambda(dx^j) \quad (32)$$

$$= \int \frac{w(x)}{w(x) + \sum_{j=2}^N w(x^j)} 1_{\mathbf{A}}(x) \prod_{j=2}^N \Lambda(dx^j) + \int \sum_{i=2}^N \frac{w(x^i)}{w(x) + \sum_{j=2}^N w(x^j)} 1_{\mathbf{A}}(x^i) \prod_{j=2}^N \Lambda(dx^j) \quad (33)$$

$$\geq \sum_{i=2}^N \int \frac{w(x^i)}{w(x) + w(x^i) + \sum_{j=2, j \neq i}^N w(x^j)} 1_{\mathbf{A}}(x^i) \prod_{j=2}^N \Lambda(dx^j) \quad (34)$$

$$\geq \sum_{i=2}^N \int \Pi(dx^i) 1_{\mathbf{A}}(x^i) \int \frac{1}{w(x) + w(x^i) + \sum_{j=2, j \neq i}^N w(x^j)} \prod_{j=2, j \neq i}^N \Lambda(dx^j). \quad (35)$$

Finally, since the function  $f: z \mapsto (z + a)^{-1}$  is convex on  $\mathbb{R}_+$  and  $a > 0$ , we get for  $i \in \{2, \dots, N\}$ ,

$$\int \frac{1}{w(x) + w(x^i) + \sum_{j=2, j \neq i}^N w(x^j)} \prod_{j=2, j \neq i}^N \Lambda(dx^j) \quad (36)$$

$$\geq \frac{1}{\int w(x) + w(x^i) + \sum_{j=2, j \neq i}^N w(x^j) \prod_{j=2, j \neq i}^N \Lambda(dx^j)} \quad (37)$$

$$\geq \frac{1}{w(x) + w(x^i) + N - 2} \geq \frac{1}{2L + N - 2}. \quad (38)$$

We finally obtain the inequality

$$\mathbf{P}_N(x, \mathbf{A}) \geq \Pi(\mathbf{A}) \times \frac{N - 1}{2L + N - 2} = \epsilon_N \Pi(\mathbf{A}). \quad (39)$$

This means that the whole space  $\mathbb{X}$  is  $(1, \epsilon_N \Pi)$ -small (see (Douc et al., 2018, Definition 9.3.5)). Since  $\mathbf{P}_N(x, \cdot)$  and  $\Pi$  are probability measures, (39) implies

$$\|\mathbf{P}_N(x, \cdot) - \Pi\|_{\text{TV}} = \sup_{\mathbf{A} \in \mathcal{X}} |\mathbf{P}_N(x, \mathbf{A}) - \Pi(\mathbf{A})| \leq 1 - \epsilon_N = \kappa_N. \quad (40)$$

Now the statement follows from (Douc et al., 2018, Theorem 18.2.4) applied with  $m = 1$ .

(ii) Let  $V: \mathbb{X} \rightarrow [1, \infty)$  be a measurable function such that  $\Pi(V) < \infty$  and  $\Lambda(V) < \infty$ . We aim to check first the drift condition

$$\mathbf{P}_N V(x) \leq \kappa_N V(x) + b_N \quad (41)$$

with the constants  $\kappa_N$  and  $b_N$  defined in Theorem 3 and (51), respectively. Setting  $x^1 = x$ , we obtain

$$\mathbf{P}_N V(x) = \int \sum_{i=1}^N \frac{w(x^i)}{\sum_{j=1}^N w(x^j)} V(x^i) \prod_{j=2}^N \Lambda(dx^j) \quad (42)$$

$$= V(x) \int \frac{w(x)}{\sum_{j=1}^N w(x^j)} \prod_{j=2}^N \Lambda(dx^j) + \int \sum_{i=2}^N \frac{w(x^i)}{\sum_{j=1}^N w(x^j)} V(x^i) \prod_{j=2}^N \Lambda(dx^j). \quad (43)$$

We bound these two terms separately.

$$V(x) \int \frac{w(x)}{\sum_{j=1}^N w(x^j)} \prod_{j=2}^N \Lambda(dx^j) = V(x) \int \left( 1 - \frac{\sum_{j=2}^N w(x^j)}{\sum_{j=1}^N w(x^j)} \right) \prod_{j=2}^N \Lambda(dx^j) \quad (44)$$

$$= V(x) \left( 1 - \sum_{k=2}^N \int \frac{w(x^k)}{w(x) + w(x^k) + \sum_{j=2, j \neq k}^N w(x^j)} \prod_{j=2}^N \Lambda(dx^j) \right) \quad (45)$$

$$= V(x) \left( 1 - \sum_{k=2}^N \int \frac{\pi(dx^k)}{w(x) + w(x^k) + \sum_{j=2, j \neq k}^N w(x^j)} \prod_{j=2, j \neq k}^N \Lambda(dx^j) \right). \quad (46)$$

From (36), we get that

$$V(x) \int \frac{w(x)}{\sum_{j=1}^N w(x^j)} \prod_{j=2}^N \Lambda(dx^j) \leq V(x) \left(1 - \frac{N-1}{2L+N-2}\right) = \kappa_N V(x). \quad (47)$$

Moreover, we have

$$\int \sum_{i=2}^N \frac{w(x^i)V(x^i)}{\sum_{j=1}^N w(x^j)} \prod_{j=2}^N \Lambda(dx^j) = (N-1) \int \frac{w(x^2)V(x^2)\Lambda(dx^2)}{w(x) + w(x^2) + \sum_{j=3}^N w(x^j)} \prod_{j=3}^N \Lambda(dx^j). \quad (48)$$

Since the function  $z \mapsto z/(z+a)$  is concave on  $\mathbb{R}_+$  for  $a > 0$ , we have

$$\begin{aligned} & \int \frac{w(x^2)}{w(x) + w(x^2) + \sum_{j=3}^N w(x^j)} V(x^2)\Lambda(dx^2) \\ &= \Lambda(V) \int \frac{w(x^2)}{w(x^2) + w(x) + \sum_{j=3}^N w(x^j)} \frac{V(x^2)\Lambda(dx^2)}{\Lambda(V)} \\ &\leq \Lambda(V) \frac{\int w(x^2)V(x^2)\Lambda(dx^2)/\Lambda(V)}{\int w(x^2)V(x^2)\Lambda(dx^2)/\Lambda(V) + w(x) + \sum_{j=3}^N w(x^j)} \leq \frac{\Pi(V)}{\Pi(V)/\Lambda(V) + w(x) + \sum_{j=3}^N w(x^j)}. \end{aligned} \quad (49)$$

Using Lemma 6, with  $Y_i = w(x^i)$ ,

$$\int \frac{\Pi(V)}{\Pi(V)/\Lambda(V) + \sum_{j=3}^N w(x^j)} \prod_{j=3}^N \Lambda(dx^j) \leq \frac{\Pi(V)}{\Pi(V)/\Lambda(V) + (N-2)/2} + \Lambda(V) \exp(-(N-2)/2L^2). \quad (50)$$

Writing in this case

$$b_N = \frac{\Pi(V)(N-1)}{\Pi(V)/\Lambda(V) + (N-2)/2} + \Lambda(V)(N-1) \exp(-(N-2)/2L^2) \quad (51)$$

concludes the proof.

Moreover, (i) implies that for any  $d_N > 1$  the level sets  $\{x \in \mathbb{X} : V(x) \leq d_N\}$  are  $(1, \epsilon_N \Pi)$ -small. Let us choose  $d_N = 1 \vee 4b_N/(1 - \kappa_N) - 1 \vee 2/\kappa_N$ . Then  $\kappa_N + 2b_N/(1 + d_N) < 1$ , and (Douc et al., 2018, Theorem 19.4.1) implies

$$\|\mathbb{P}_N^n(x, \cdot) - \Pi\|_V \leq c_N \{V(x) + \Pi(V)\} \tilde{\kappa}_N^n, \quad (52)$$

where the constants  $\tilde{\kappa}_N$  and  $c_N$  are given by

$$\log \tilde{\kappa}_N = \frac{\log \kappa_N \log \bar{\lambda}_N}{(\log \kappa_N + \log \bar{\lambda}_N - \log \bar{b}_N)}, \quad c_N = (\bar{\lambda}_N + 1)(1 + \bar{b}_N/[\kappa_N(1 - \bar{\lambda}_N)]) \quad (53)$$

$$\bar{\lambda}_N = \kappa_N + 2b_N/(1 + d_N), \quad \bar{b}_N = \kappa_N b_N + d_N, \quad d_N = 1 \vee 4b_N/(1 - \kappa_N) - 1 \vee 2/\kappa_N. \quad (54)$$

In the expression above we used the fact that  $1 - \epsilon_N = \kappa_N$ . The choice of  $d_N$  in (53) implies  $2b_N/(1 + d_N) \leq b_N \kappa_N$ . Then the elementary calculations imply  $\kappa_N \leq \bar{\lambda}_N \leq (b_N + 1)\kappa_N$  and

$$\tilde{\kappa}_N \leq \kappa_N^{\theta_N}, \quad (55)$$

where

$$\theta_N = \frac{\log(1/\bar{\lambda}_N)}{(\log(1/\kappa_N) + \log(1/\bar{\lambda}_N) + \log \bar{b}_N)} \geq \frac{\log(1/\kappa_N) - \log(b_N + 1)}{2 \log(1/\kappa_N) + \log \bar{b}_N} = \frac{1}{3} + \alpha_N. \quad (56)$$

In the expression above  $\alpha_N \rightarrow 0$  when  $N \rightarrow \infty$ , since  $b_N \leq 4\Pi(V)$  for  $N \geq 3$ .  $\square$

### B.3 Proof of Theorem Theorem 4

We preface the proof with some preparatory lemmas.

**Lemma 7.** *Let  $K \subset \mathbb{X}$ , such that  $\sup_{x \in K} w(x) < w_{\infty, K} < \infty$  and  $\Pi(K) > 0$ . Then, for all  $(x, A) \in K \times \mathcal{X}$ ,*

$$P_N(x, A) \geq \epsilon_{N, K} \Pi_K(A), \quad (57)$$

with  $\epsilon_{N, K} = (N-1)\Pi(K)/[2w_{\infty, K} + N - 2]$  and  $\Pi_K(A) = \Pi(A \cap K)/\Pi(K)$ .

Note that if the weight function  $w$  is continuous, then for any compact  $K$ ,  $\sup_{x \in K} w(x) < w_{\infty, K} < \infty$ .

*Proof.* Let  $(x, A) \in \mathbb{X} \times \mathcal{X}$ . Then

$$P_N(x, A) = \int \frac{w(x)}{w(x) + \sum_{j=2}^N w(x^j)} 1_A(x) \prod_{j=2}^N \Lambda(dx^j) + \int \sum_{i=2}^N \frac{w(x^i)}{w(x) + \sum_{j=2}^N w(x^j)} 1_A(x^i) \prod_{j=2}^N \Lambda(dx^j) \quad (58)$$

$$\geq \sum_{i=2}^N \int \frac{w(x^i)}{w(x) + w(x^i) + \sum_{j=2, j \neq i}^N w(x^j)} 1_A(x^i) \prod_{j=2}^N \Lambda(dx^j) \quad (59)$$

$$\geq \sum_{i=2}^N \int \Pi(dx^i) 1_A(x^i) \int \frac{1}{w(x) + w(x^i) + \sum_{j=2, j \neq i}^N w(x^j)} \prod_{j=2, j \neq i}^N \Lambda(dx^j) \quad (60)$$

$$\geq (N-1) \int \Pi(dx^1) 1_A(x^1) \frac{1}{w(x) + w(x^1) + N-2}, \quad (61)$$

where the last inequality follows from Jensen's inequality and the convexity of the function  $z \mapsto (z+a)^{-1}$  on  $\mathbb{R}_+$ . Now,

$$P_N(x, A) \geq (N-1) \int \Pi(dx^1) 1_{A \cap K}(x^1) \frac{1}{w(x) + w(x^1) + N-2} \quad (62)$$

$$\geq \frac{N-1}{2w_{\infty, K} + N-2} \int \Pi(dy) 1_{A \cap K}(y) = \frac{(N-1)\Pi(K)}{2w_{\infty, K} + N-2} \Pi_K(A). \quad (63)$$

□

**Lemma 8.** *Let  $P$  be a Markov kernel on  $(\mathbb{X}, \mathcal{X})$ ,  $\gamma$  be a probability measure on  $(\mathbb{X}, \mathcal{X})$ , and  $\epsilon > 0$ . Let also  $C \in \mathcal{X}$  be an  $(1, \epsilon\gamma)$ -small set for  $P$ . Then for arbitrary Markov kernel  $Q$  on  $(\mathbb{X}, \mathcal{X})$ , the set  $C$  is an  $(1, \epsilon\gamma_Q)$ -small set for  $PQ$ , where  $\gamma_Q(A) = \int \gamma(dy)Q(y, A)$  for  $A \in \mathcal{X}$ .*

*Proof.* Let  $(x, A) \in C \times \mathcal{X}$ . Then it holds

$$PQ(x, A) = \int P(x, dy)Q(y, A) \geq \epsilon \int_C \gamma(dy)P(y, A) = \epsilon\gamma(A). \quad (64)$$

□

**Lemma 9.** *Let  $P$  and  $Q$  be two irreducible Markov kernels with  $\Pi$  as their unique invariant distribution. Let  $V : \mathbb{X} \rightarrow [1, \infty)$  be a measurable function. Assume that there exists  $\lambda_Q \in [0, 1)$  and  $b_P, b_Q \in \mathbb{R}_+$  such that  $PV(x) \leq V(x) + b_P$  and  $QV(x) \leq \lambda_Q V(x) + b_Q$ . Let  $d_0 > 1$ . Assume in addition, that for all  $d \geq d_0$ , there exist  $\epsilon_d > 0$  and a probability measure  $\gamma_d$  such that for all  $(x, A) \in V_d \times \mathcal{X}$ ,  $P(x, A) \geq \epsilon_d \gamma_d(A)$ , where  $V_d = \{x \in \mathbb{X} : V(x) \leq d\}$ . Define  $K = PQ$  and  $\lambda_K = \lambda_Q$ ,  $b_K = b_P + b_Q$ . Then,*

$$KV(x) \leq \lambda_K V + b_K \text{ and, for all } x \in V_d, K(x, A) \geq \epsilon_d \gamma_{Q,d}(A),$$

where  $\gamma_{Q,d}(A) = \int \gamma_d(dy)Q(y, A)$ .

Let  $d \geq d_0$  be such that  $\lambda_K + 2b_K/(1+d) < 1$ . Then, for any  $x \in \mathbb{X}$  and  $k \in \mathbb{N}$ ,

$$\|K^k(x, \cdot) - \Pi\|_V \leq c_K \{V(x) + \Pi(V)\} \rho_K^k$$

with

$$\rho_K = \frac{\log(1 - \epsilon_d) \log \bar{\lambda}_K}{\log(1 - \epsilon_d) + \log \bar{\lambda}_K - \log \bar{b}_K}, \quad (65)$$

with  $\bar{\lambda}_K = \lambda_K + 2b_K/(1 + d)$ ,  $\bar{b}_K = \lambda_K b_K + d$ , and  $c_K = (\lambda_K + 1)(1 + \bar{b}_K)/[(1 - \epsilon_{V_d})(1 - \bar{\lambda}_K)]$ .

*Proof.* By Lemma 8, we have directly that for any  $(x, A) \in V_d \times \mathcal{X}$ ,  $K(x, A) \geq \epsilon_d \gamma_{Q,d}(A)$ . Moreover, for any  $x \in \mathbb{X}$ ,  $KV(x) = PQV(x) \leq \lambda_Q PV(x) + b_Q \leq \lambda_Q V(x) + b_Q + b_P$ . The proof is completed with (Douc et al., 2018, Theorem 19.4.1).  $\square$

*Proof of Theorem 10.* Note first, that the Markov kernel of Ex<sup>2</sup>MCMC algorithm can be represented as a composition  $K_N = P_N R$  with  $R$  being the rejuvenation kernel. Applying the same symmetrisation argument as (23), we write  $K_N$  for  $(x, A) \in \mathbb{X} \times \mathcal{X}$  as

$$K_N(x, A) = \frac{1}{N} \int \sum_{\ell=1}^N \delta_x(dx_\ell) \prod_{i \neq \ell} \Lambda(dx^i) \sum_{i=1}^N \frac{w(x^i)}{\sum_{\ell=1}^N w(x^\ell)} R(x^i, A). \quad (66)$$

Applying (42)-(48)-(49), we get

$$P_N V(x) = V(x) \int \frac{w(x)}{w(x) + \sum_{j=2}^N w(x^j)} \prod_{j=2}^N \Lambda(dx^j) + \int \sum_{i=2}^N \frac{w(x^i)}{\sum_{j=1}^N w(x^j)} V(x^i) \prod_{j=2}^N \Lambda(dx^j) \quad (67)$$

$$\leq V(x) + (N-1)U_N \quad \text{with} \quad U_N = \int \frac{\Pi(V)}{\Pi(V)/\Lambda(V) + w(x) + \sum_{j=3}^N w(x^j)} \prod_{j=3}^N \Lambda(dx^j) \quad (68)$$

On the other hand, using (29) with  $K = (N-2)/2$  together with Markov inequality,

$$U_N \leq \frac{\Pi(V)}{\Pi(V)/\Lambda(V) + (N-2)/2} + \Lambda(V) \int 1_{\{\sum_{j=3}^N \{w(x^j)-1\} \leq -(N-2)/2\}} \prod_{j=3}^N \Lambda(dx^j), \quad (69)$$

$$\leq \frac{\Pi(V)}{\Pi(V)/\Lambda(V) + (N-2)/2} + \frac{4\Lambda(V) \text{Var}_\Lambda[w]}{N-2}, \quad (70)$$

where  $\text{Var}_\Lambda[w] = \int \{w(x) - 1\}^2 \Lambda(dx)$  is the variance of the normalized weight functions under the proposal distribution. Combining the above results, for any  $x \in \mathbb{X}$ ,

$$P_N V(x) \leq V(x) + b_{P_N}, \quad \text{where } b_{P_N} = \frac{\Pi(V)(N-1)}{\Pi(V)/\Lambda(V) + (N-2)/2} + \frac{4(N-1)\Lambda(V) \text{Var}_\Lambda[w]}{N-2}. \quad (71)$$

Assumption **A2-(i)** implies  $RV(x) \leq \lambda_R V(x) + b_R$ . Assumption **A2** together with Lemma 7 implies that the level sets  $V_d$  are  $(1, \epsilon_{d,N} \gamma_d)$ -small for the Markov kernel  $P_N$ . Here the probability measure  $\gamma_d$  and  $\epsilon_{d,N}$  are given, for any  $A \in \mathcal{X}$ , by

$$\begin{aligned} \gamma_d(A) &= \int \Pi_{V_d}(dy) R(y, A), \quad \text{where } \Pi_{V_d}(B) = \Pi(B \cap V_d)/\Pi(V_d), B \in \mathcal{X}, \\ \epsilon_{d,N} &= (N-1)\Pi(V_d)/[2w_{\infty,d} + N-2]. \end{aligned} \quad (72)$$

Hence all conditions of Lemma 9 are satisfied. Choose  $d_N = 1 \vee 4(b_R + b_{P_N})/(1 - \lambda_R) - 1$ . Then  $\lambda_R + 2(b_R + b_{P_N})/(1 + d_N) < 1$ , and Lemma 9 implies for any  $x \in \mathbb{X}$  and  $k \in \mathbb{N}$ ,

$$\|K_N^k(x, \cdot) - \Pi\|_V \leq c_{N,R} \{V(x) + \Pi(V)\} \tilde{\kappa}_{N,R}^k,$$

where the constants  $c_{N,R}$  and  $\tilde{\kappa}_{N,R}$  are given by

$$\log \tilde{\kappa}_{N,R} = \frac{\log(1 - \epsilon_{d,N}) \log \bar{\lambda}_R}{\log(1 - \epsilon_{d,N}) + \log \bar{\lambda}_R - \log \bar{b}_R}, \quad c_{N,R} = (\lambda_R + 1)(1 + \bar{b}_R)/[(1 - \epsilon_{d,N})(1 - \bar{\lambda}_R)] \quad (73)$$

$$\bar{\lambda}_R = \lambda_R + 2b_R/(1 + d), \quad \bar{b}_R = \lambda_R b_R + d_N, \quad d_N = 1 \vee 4(b_R + b_{P_N})/(1 - \lambda_R) - 1, \quad (74)$$

and  $\epsilon_{d,N}$  defined in (72). It is easy to see from this expression that, for  $d_N$  being fixed,  $\tilde{\kappa}_{N,R}$  decreases with  $N \rightarrow \infty$ .  $\square$

#### B.4 Proof of Theorem Theorem 5

The algorithm Ex<sup>2</sup>MCMC defines a Markov chain  $\{Y_j, j \in \mathbb{N}\}$  with Markov kernel

$$C_N(x, A) = \frac{1}{N} \int \sum_{j=1}^N \delta_x(dx^j) Q_j(x^j, dx^{1:N \setminus \{j\}}) \times \sum_{i=1}^N \frac{w(x^i)}{\sum_{\ell=1}^N w(x^\ell)} R(x^i, A). \quad (75)$$

Let  $f$  be a nonnegative measurable function. Using that  $\Pi(dy)\delta_y(dx^j) = \Pi(dx^j)\delta_{x^j}(dy)$ ,  $\Pi(dx^j) = \Lambda(dx^j)w(x^j)$ , and  $\Lambda(dx^j)Q_j(x^j, dx^{1:N \setminus \{j\}}) = \bar{\Lambda}_N(dx^{1:N})$ , we get

$$\int \Pi(dy)C_N(y, dy')f(y') = N^{-1} \int \sum_{j=1}^N w(x^j) \bar{\Lambda}_N(dx^{1:N}) \sum_{i=1}^N \frac{w(x^i)}{\sum_{\ell=1}^N w(x^\ell)} Rf(x^i) \quad (76)$$

$$= N^{-1} \int \sum_{i=1}^N w(x^i) Rf(x^i) \bar{\Lambda}_N(dx^{1:N}). \quad (77)$$

Using that

$$w(x^i) \bar{\Lambda}_N(dx^{1:N}) = w(x^i) \Lambda(dx^i) Q_j(x^j, dx^{1:N \setminus \{j\}}) = \Pi(dx^i) Q_i(x^i, dx^{1:N \setminus \{i\}}), \quad (78)$$

we obtain

$$\begin{aligned} N^{-1} \int \sum_{i=1}^N w(x^i) Rf(x^i) \bar{\Lambda}_N(dx^{1:N}) &= N^{-1} \sum_{i=1}^N \Pi(dx^i) Rf(x^i) Q_i(x^i, dx^{1:N \setminus \{i\}}) \\ &= \sum_{i=1}^N \int \Pi(dx^i) f(x^i) \int Q_i(x^i, dx^{1:N \setminus \{i\}}) = \int \Pi(dy) f(y), \end{aligned} \quad (79)$$

where we have used  $\int Q_i(x^i, dx^{1:N \setminus \{i\}}) = 1$ .

### C Metropolis-Adjusted Langevin rejunevation kernel

Assume that  $\mathbb{X} = \mathbb{R}^d$  and the target distribution  $\Pi$  is absolutely continuous with  $\Pi(dx) = \pi(x)dx$ , where  $\pi(x) = \exp\{-U(x)\}$  with continuously differentiable function  $U(x)$ . Then the MALA kernel is given, for  $\gamma > 0$ ,  $x, z \in \mathbb{R}^d$ , and  $A \in \mathcal{B}(\mathbb{R}^d)$ , by

$$R_\gamma^{\text{MALA}}(x, A) = \int_{\mathbb{R}^d} 1_A(x - \gamma \nabla U(x) + \sqrt{2\gamma}z) \min(1, e^{-\tau_\gamma^{\text{MALA}}(x, z)}) \varphi(z) dz \quad (80)$$

$$\delta_x(A) \int_{\mathbb{R}^d} \{1 - \min(1, e^{-\tau_\gamma^{\text{MALA}}(x, z)})\} \varphi(z) dz,$$

$$\tau_\gamma^{\text{MALA}}(x, z) = U(x - \gamma \nabla U(x) + \sqrt{2\gamma}z) - U(x) \quad (81)$$

$$+ (1/2) \{ \|z - (\gamma/2)^{1/2} \{ \nabla U(x) + \nabla U(x - \gamma \nabla U(x) + \sqrt{2\gamma}z) \} \|^2 - \|z\|^2 \}. \quad (82)$$

Note that the MALA kernel leaves the target  $\pi$  invariant. For notation simplicity, in this section we simply write  $R_\gamma$  instead of  $R_\gamma^{\text{MALA}}$ . Consider the following assumptions on the target distribution:

**H 1.**  $U(x) \in C_{\text{poly}}^\infty(\mathbb{R}^d, \mathbb{R})$ , and  $\nabla U$  is Lipschitz, i.e. there exists  $L \geq 0$  such that  $\|\nabla U(x) - \nabla U(y)\| \leq L\|x - y\|$  for all  $x, y \in \mathbb{R}^d$ .

**H 2.** There exist  $K_1 \geq 0$  and  $m > 0$  such that for any  $x \notin B(0, K_1)$ , and  $y \in \mathbb{R}^d$ ,  $\langle D^2 U(x)y, y \rangle \geq m\|y\|^2$ . Moreover, there exists  $M \geq 0$  such that for any  $x \in \mathbb{R}^d$ ,  $\|D^3 U(x)\| \leq M$ .

**Theorem 10.** Assume **H 1**, **H 2** and that the proposal distribution has a continuous and positive p.d.f.  $\Lambda(x)$ . Then **A 2** is satisfied with  $V(x) = \exp(\bar{\eta}\|x\|^2)$ ,  $\bar{\eta}$  given in (95).

*Proof.* Proposition 18 implies that **A 2**-(ii) holds. Assume H1 and H2. Then there exist  $\bar{\gamma} > 0$ ,  $\varpi > 0$ , and  $K_2, \bar{b} \geq 0$  such that for any  $\gamma \in (0, \bar{\gamma}]$  and  $x \in \mathbb{R}^d$ ,

$$R_\gamma V_{\bar{\eta}}(x) \leq \lambda_{R_\gamma} V_{\bar{\eta}}(x) + b_{R_\gamma}, \text{ where } \lambda_{R_\gamma} = 1 - \varpi\gamma, b_{R_\gamma} = \bar{b}\gamma, \quad (83)$$

and the parameters  $\varpi$  and  $\bar{b}$  are given in (135). Moreover, since  $\Lambda$  and  $\Pi$  are continuous and  $\Lambda(x) > 0$ , the weight function  $w(x)$  is bounded on the compact sets and **A2-(iii)** holds. Hence, all conditions of Lemma 9 are satisfied.  $\square$

Consider now the sampling problem described in Appendix F.4. We state the following result.

**Proposition 11.** *Let  $\pi(x) = g(x; 0, \text{Id}_D)$  and  $\lambda(x) = g(x; 0, 2\text{Id}_D)$ . Let  $V_{\bar{\eta}}(x) = \exp(\bar{\eta}\|x\|^2)$ , where  $\bar{\eta}$  is given in (95). Then, for  $N \geq e^{2\bar{\eta}D}$ , the Markov kernel of Ex<sup>2</sup>MCMC algorithm with MALA rejuvenation kernel satisfies*

$$\|\mathbf{K}_N^k(x, \cdot) - \Pi\|_V \leq c_K \{V_{\bar{\eta}}(x) + \Pi(V_{\bar{\eta}})\} \tilde{\kappa}_{N,R}^k, \text{ where } \log \tilde{\kappa}_{N,R} \leq \frac{\log(1 - \varpi\gamma)}{1 + 8\bar{\eta}} + \alpha_N, \quad (84)$$

and  $\alpha_N \rightarrow 0$  for  $N \rightarrow \infty$ , and  $c_K$  is given in (74).

*Proof.* From the proof of Theorem 10, it follows that

$$\|\mathbf{K}_N^k(x, \cdot) - \Pi\|_V \leq c_{N,R} \{V(x) + \Pi(V)\} \tilde{\kappa}_{N,R}^k,$$

where the constants  $c_{N,R}$  and  $\tilde{\kappa}_{N,R}$  are given in (74). We first estimate the quantity  $\epsilon_{d_N, N} = (N - 1)\Pi(V_{d_N})/[2w_{\infty, d_N} + N - 2]$ . Note that

$$w_{\infty, d_N} \leq \sup_{x \in \mathbb{R}^D} \frac{\pi(x)}{\lambda(x)} = 2^{D/2},$$

which does not depend on the choice of  $d_N$ . Hence, for any choice  $d_N$ ,  $\epsilon_{d_N, N}/\Pi(V_{d_N}) \rightarrow 1$  as  $N \rightarrow \infty$ . Now we can lower bound  $\Pi(V_{d_N})$  as follows. Note that  $V_{d_N} = \{x \in \mathbb{X} : V_{\bar{\eta}}(x) \leq d_N\} = \{x \in \mathbb{X} : \|x\|^2 \leq \log d_N/\bar{\eta}\}$ . Then, for  $\log d_N/\bar{\eta} \geq 2D$ , we write

$$\Pi(V_{d_N}) = \mathbb{P} \left( \|Z\|^2 \leq \left( \frac{\log d_N}{\bar{\eta}} - D \right) + D \right) \geq 1 - \exp \left\{ - \frac{\log d_N}{8\bar{\eta}} + \frac{D}{8} \right\}, \quad (85)$$

where  $Z = (Z_1, \dots, Z_D) \sim \Pi$ . Here we use the fact that  $\|Z\|^2$  is a chi-squared random variable with  $D$  degrees of freedom and (Wainwright, 2019, Proposition 2.2). Hence,  $\log(1 - \epsilon_{d_N, N}) \leq -\left(\frac{\log d_N}{8\bar{\eta}} - \frac{D}{8}\right)$ . Then using the expression (74) and choosing

$$d_N = 1 \vee 4(b_R + b_{P_N})/(1 - \lambda_R) - 1 \vee N \vee e^{2\bar{\eta}D}, \quad (86)$$

we have

$$\log \tilde{\kappa}_{N,R} = \frac{\log(1 - \epsilon_{d_N, N}) \log \bar{\lambda}_R}{\log(1 - \epsilon_{d_N, N}) + \log \bar{\lambda}_R - \log \bar{b}_R} = \frac{\log \bar{\lambda}_R}{1 + \log \bar{\lambda}_R / \log(1 - \epsilon_{d_N, N}) - \log \bar{b}_R / \log(1 - \epsilon_{d_N, N})}. \quad (87)$$

Note that  $\log \bar{\lambda}_R / \log(1 - \epsilon_{d_N, N}) \rightarrow 0$ ,  $N \rightarrow \infty$ . Now the statement follows from  $\log \bar{b}_R / \log(1 - \epsilon_{d_N, N}) = -8\bar{\eta} + \beta_N$ ,  $\beta_N \rightarrow 0$  for  $N \rightarrow \infty$ .  $\square$

## D Technical lemmas for Metropolis-Adjusted Langevin kernel

The goal of this section is to establish the Foster-Lyapunov drift condition for the Markov kernel  $R_\gamma^{\text{MALA}}$  defined in (80). As an auxiliary result we need to establish the drift condition for the Markov kernel  $Q_\gamma^{\text{ULA}}$ , defined as

$$Q_\gamma^{\text{ULA}}(x, A) = \int_{\mathbb{R}^d} 1_A \left( x - \gamma \nabla U(x) + \sqrt{2\gamma} z \right) \varphi(z) dz, \quad (88)$$

where  $\varphi$  is the  $d$ -dimensional standard Gaussian density  $\varphi(z) = (2\pi)^{-d/2} e^{-\|z\|^2}$ . Define for any  $\eta > 0$ ,  $V_\eta(x) : \mathbb{R}^d \rightarrow [1, +\infty)$  as

$$V_\eta(x) = \exp(\eta\|x\|^2). \quad (89)$$

For notation simplicity, we write in this section  $Q_\gamma$  instead of  $Q_\gamma^{\text{ULA}}$ , and  $R_\gamma$  instead of  $R_\gamma^{\text{MALA}}$ . We begin with the technical lemma.

**Lemma 12.** *Assume H1 and H2. Then there exists  $K_2 \geq 0$  such that for any  $x \notin B(0, K_2)$ ,  $\langle \nabla U(x), x \rangle \geq (m/2)\|x\|^2$  and in particular  $\|\nabla U(x)\| \geq (m/2)\|x\|$ .*

*Proof.* Using H1 and H2, we have for any  $x \in \mathbb{R}^d$ ,  $\|x\| \geq K_1$ ,

$$\langle \nabla U(x), x \rangle = \int_0^{K_1/\|x\|} D^2 U(tx)[x^{\otimes 2}] dt + \int_{K_1/\|x\|}^1 D^2 U(tx)[x^{\otimes 2}] dt \quad (90)$$

$$\geq m\|x\|^2\{1 - K_1(1 + L/m)/\|x\|\}, \quad (91)$$

which proves the first statement. The second statement easily follows from the Cauchy-Schwartz inequality.  $\square$

**Lemma 13.** *Assume H1 and H2. Then, for any  $t \in [0, 1]$ ,  $\gamma \in (0, 1/(4L)]$  and  $x, z \in \mathbb{R}^d$ ,  $\|z\| \leq \|x\|/(4\sqrt{2\gamma})$ , it holds*

$$\|x + t\{-\gamma \nabla U(x) + \sqrt{2\gamma}z\}\| \geq \|x\|/2. \quad (92)$$

*Proof.* Let  $t \in [0, 1]$ ,  $\gamma \in (0, 1/(4L)]$  and  $x, z \in \mathbb{R}^d$ ,  $\|z\| \leq \|x\|/(4\sqrt{2\gamma})$ . Using the triangle inequality and H1, we have since  $t \in [0, 1]$

$$\|x + t\{-\gamma \nabla U(x) + \sqrt{2\gamma}z\}\| \geq (1 - \gamma L)\|x\| - \sqrt{2\gamma}\|z\|. \quad (93)$$

The conclusion then follows from  $\gamma \leq 1/(4L)$  and  $\|z\| \leq \|x\|/(4\sqrt{2\gamma})$ .  $\square$

Now we establish the drift condition for  $Q_\gamma^{\text{ULA}}$ .

**Lemma 14.** *Assume H1 and H2, and let  $\bar{\gamma} \in (0, m/(4L^2)]$ . Then, for any  $\gamma \in (0, \bar{\gamma}]$ ,*

$$Q_\gamma V_{\bar{\eta}}(x) \leq \exp(-\bar{\eta}m\gamma\|x\|^2/4) V_{\bar{\eta}}(x) + b_{\bar{\eta}}\gamma 1_{B(0, K_3)}(x), \quad (94)$$

where  $V_{\bar{\eta}}$  is defined by (89),  $\bar{\eta} = \min(m/16, (8\bar{\gamma})^{-1})$ ,  $K_3 = \max(K_2, 4\sqrt{d/m})$ , and

$$\begin{aligned} b_{\bar{\eta}} = & [\bar{\eta} \{m/4 + (1 + 16\bar{\eta}\bar{\gamma})(4\bar{\eta} + 2L + \bar{\gamma}L^2)\} K_3^2 + 4\bar{\eta}d] \\ & \times \exp[\bar{\gamma}\bar{\eta} \{m/4 + (1 + 16\bar{\eta}\bar{\gamma})(4\bar{\eta} + 2L + \bar{\gamma}L^2)\} K_3^2 + (d/2)\log(2)]. \end{aligned} \quad (95)$$

*Proof.* Let  $\gamma \in (0, \bar{\gamma}]$ . For any  $x \in \mathbb{R}^d$ , we have

$$\bar{\eta}\|x - \gamma \nabla U(x) + \sqrt{2\gamma}z\|^2 - \|z\|^2/2 = -\frac{1 - 4\bar{\eta}\gamma}{2}\|z - \frac{2(2\gamma)^{1/2}\bar{\eta}}{1 - 4\bar{\eta}\gamma}\{x - \gamma \nabla U(x)\}\|^2 + \frac{\bar{\eta}}{1 - 4\bar{\eta}\gamma}\|x - \gamma \nabla U(x)\|^2. \quad (96)$$

Since  $1 - 4\bar{\eta}\gamma > 0$ , we get that

$$\begin{aligned} Q_\gamma V_{\bar{\eta}}(x) &= (2\pi)^{-d/2} \int_{\mathbb{R}^d} \exp\left(\bar{\eta}\|x - \gamma \nabla U(x) + \sqrt{2\gamma}z\|^2 - \|z\|^2/2\right) dz \\ &= (1 - 4\bar{\eta}\gamma)^{-d/2} \exp(\bar{\eta}(1 - 4\bar{\eta}\gamma)^{-1}\|x - \gamma \nabla U(x)\|^2). \end{aligned} \quad (97)$$

We now distinguish the case when  $\|x\| \geq K_3$  and  $\|x\| < K_3$ . By H2 and Lemma 12, for any  $x \in \mathbb{R}^d$ ,  $\|x\| \geq K_3 \geq K_2$ , using that  $\bar{\eta} \leq m/16$  and  $\gamma \leq \bar{\gamma} \leq m/(4L^2)$ , we have

$$(1 - 4\bar{\eta}\gamma)^{-1}\|x - \gamma \nabla U(x)\|^2 - \|x\|^2 \leq \gamma\|x\|^2(1 - 4\bar{\eta}\gamma)^{-1}(4\bar{\eta} - m + \gamma L^2) \leq -\gamma(m/2)\|x\|^2(1 - 4\bar{\eta}\gamma)^{-1}. \quad (98)$$

Therefore, (97) becomes

$$Q_\gamma V_{\bar{\eta}}(x) \leq \exp(-\gamma\bar{\eta}(m/2)(1 - 4\bar{\eta}\gamma)^{-1}\|x\|^2 - (d/2)\log(1 - 4\bar{\eta}\gamma)) V_{\bar{\eta}}(x) \quad (99)$$

$$\leq \exp(\gamma\bar{\eta}\{-(m/2)\|x\|^2 + 4d\}) V_{\bar{\eta}}(x), \quad (100)$$

where we have used for the last inequality that  $-\log(1 - t) \leq 2t$  for  $t \in [0, 1/2]$  and  $4\bar{\eta}\gamma \leq 1/2$ . The proof of the statement then follows since  $\|x\| \geq K_3 \geq 4\sqrt{d/m}$ .  $\square$

In the case  $\|x\| < K_3$ , by (97), H1 and since  $(1-t)^{-1} \leq 1+4t$  for  $t \in [0, 1/2]$ , we obtain

$$(1-4\bar{\eta}\gamma)^{-1}\|x - \gamma\nabla U(x)\|^2 - \|x\|^2 \leq \gamma(1-4\bar{\eta}\gamma)^{-1}\{4\bar{\eta} + 2L + \gamma L^2\}\|x\|^2 \quad (101)$$

$$\leq \gamma(1+16\bar{\eta}\gamma)\{4\bar{\eta} + 2L + \gamma L^2\}\|x\|^2, \quad (102)$$

which implies that

$$Q_\gamma V_{\bar{\eta}}(x)/V_{\bar{\eta}}(x) \leq e^{-\bar{\eta}m\gamma\|x\|^2/4} + \exp\left[\gamma\bar{\eta}\left\{m/4 + (1+16\bar{\eta}\gamma)(4\bar{\eta} + 2L + \gamma L^2)\right\}\|x\|^2 - (d/2)\log(1-4\bar{\eta}\gamma)\right] - 1. \quad (103)$$

The proof is then completed using that for any  $t \geq 0$ ,  $e^t - 1 \leq te^t$ , for any  $s \in [0, 1/2]$ ,  $-\log(1-s) \leq 2s$  and  $4\bar{\eta}\gamma \leq 1/2$ .  $\square$

We now provide a decomposition in  $\gamma$  of  $\tau_\gamma^{\text{MALA}}$  defined in (81). For any  $x, z \in \mathbb{R}^d$ , by (Durmus et al., 2017, Lemma 24)<sup>1</sup>, we have that

$$\tau_\gamma^{\text{MALA}}(x, z) = \sum_{k=2}^6 \gamma^{k/2} A_{k,\gamma}(x, z) \quad (104)$$

where, setting  $x_t = x + t\{-\gamma\nabla U(x) + \sqrt{2\gamma}z\}$ ,

$$A_{2,\gamma}(x, z) = 2 \int_0^1 D^2 U(x_t)[z^{\otimes 2}](1/2-t)dt \quad (105)$$

$$A_{3,\gamma}(x, z) = 2^{3/2} \int_0^1 D^2 U(x_t)[z \otimes \nabla U(x)](t-1/4)dt, \quad (106)$$

$$A_{4,\gamma}(x, z) = - \int_0^1 D^2 U(x_t)[\nabla U(x)^{\otimes 2}]tdt + (1/2)\left\| \int_0^1 D^2 U(x_t)[z]dt \right\|^2 \quad (107)$$

$$A_{5,\gamma}(x, z) = -(1/2)^{1/2} \left\langle \int_0^1 D^2 U(x_t)[\nabla U(x)]dt, \int_0^1 D^2 U(x_t)[z]dt \right\rangle \quad (108)$$

$$A_{6,\gamma}(x, z) = (1/4)\left\| \int_0^1 D^2 U(x_t)[\nabla U(x)]dt \right\|^2. \quad (109)$$

**Lemma 15.** *Assume H1 and H2. Then, for any  $\bar{\gamma} > 0$ , there exists  $C_{1,\bar{\gamma}} < \infty$  such that for any  $x, z \in \mathbb{R}^d$ ,  $\gamma \in (0, \bar{\gamma}]$ , it holds*

$$|\tau_\gamma^{\text{MALA}}(x, z)| \leq C_{1,\bar{\gamma}}\gamma^{3/2}\{1 + \|z\|^4 + \|x\|^2\}. \quad (110)$$

*Proof.* Since  $\int_0^1 D^2 U(x)[z^{\otimes 2}](1/2-t)dt = 0$ , we get setting  $x_t = x + t\{-\gamma\nabla U(x) + \sqrt{2\gamma}z\}$ ,

$$\begin{aligned} A_{2,\gamma}(x, z) &= \sqrt{\gamma} \int_0^1 D^3 U(sx_t + (1-s)x) \left[ z^{\otimes 2} \otimes \{-\gamma^{1/2}\nabla U(x) + \sqrt{2}z\} \right] (1/2-t)tdsdt. \end{aligned} \quad (111)$$

The proof follows from  $\sup_{x \in \mathbb{R}^d} \|D^2 U(x)\| \leq L$  and  $\sup_{x \in \mathbb{R}^d} \|D^3 U(x)\| \leq M$ .  $\square$

**Lemma 16.** *Assume H1 and H2. Then, for any  $\bar{\gamma} \in (0, m^3/(4L^4)]$  there exists  $C_{2,\bar{\gamma}} < \infty$  such that for any  $\gamma \in (0, \bar{\gamma}]$ ,  $x, z \in \mathbb{R}^d$  satisfying  $\|x\| \geq \max(2K_1, K_2)$  and  $\|z\| \leq \|x\|/(4\sqrt{2\gamma})$ , where  $K_2$  is defined in Lemma 12, it holds*

$$\tau_\gamma^{\text{MALA}}(x, z) \leq C_{2,\bar{\gamma}}\gamma\|z\|^2\{1 + \|z\|^2\}. \quad (112)$$

*Proof.* Let  $\gamma \in (0, \bar{\gamma}]$ ,  $x, z \in \mathbb{R}^d$  satisfying  $\|x\| \geq \max(2K_1, K_2)$  and  $\|z\| \leq \|x\|/(4\sqrt{2\gamma})$ . Using (104), we get setting

$$A_{4,0,\gamma}(x, z) = \int_0^1 D^2 U(x_t)[\nabla U(x)^{\otimes 2}]tdt,$$

<sup>1</sup>Note that with the notation of Durmus et al. (2017), MALA corresponds to HMC with only one leapfrog step and step size equals to  $(2\gamma)^{1/2}$

$$\begin{aligned}\tau_{\gamma}^{\text{MALA}}(x, z) &\leq 2\gamma A_{2,\gamma}(x, z) - \gamma^2 A_{4,0,\gamma}(x, z) \\ &\quad + (2\gamma)^{3/2} L^2 \|z\| \|x\| + (\gamma^2/2) L^2 \|z\|^2 + (\gamma^5/2)^{1/2} L^3 \|z\| \|x\| + (\gamma^3/4) L^4 \|x\|^2,\end{aligned}\quad (113)$$

By H1, Lemma 12 and Lemma 13, we get for any  $x \in \mathbb{R}^d$ ,  $\|x\| \geq \max(2K_1, K_2)$ ,

$$A_{4,0,\gamma}(x, z) \geq (m/2)^3 \|x\|^2. \quad (114)$$

Combining this result with (111), (114) in (113), we obtain using  $\gamma \leq \bar{\gamma} \leq m^3/(4L^4)$

$$\tau_{\gamma}^{\text{MALA}}(x, z) \leq 2\gamma M \left\{ \sqrt{2\bar{\gamma}} \|z\|^3 + \gamma L \|z\|^2 \|x\| \right\} - \gamma^2 (m^3/2^4) \|x\|^2 \quad (115)$$

$$+ (2\gamma)^{3/2} L^2 \|z\| \|x\| + (\gamma^2/2) L^2 \|z\|^2 + (\gamma^5/2)^{1/2} L^3 \|z\| \|x\|, \quad (116)$$

Since for any  $a, b \in \mathbb{R}^+$  and  $\varepsilon > 0$ ,  $ab \leq (\varepsilon/2)a^2 + 1/(2\varepsilon)b^2$ , we obtain

$$\tau_{\gamma}^{\text{MALA}}(x, z) \leq \gamma \|z\|^2 \left\{ 2^{1/2} L^2 \varepsilon^{-1} + (\gamma/2) L^2 + 2^{-3/2} \gamma^{3/2} L^3 \varepsilon^{-1} \right\} \quad (117)$$

$$+ (2^3 \gamma)^{1/2} M \|z\| + \gamma M L \varepsilon^{-1} \|z\|^2 \quad (118)$$

$$+ \|x\|^2 \gamma^2 \left[ \varepsilon \left\{ LM + 2^{1/2} L^2 + 2^{-3/2} \bar{\gamma}^{1/2} L^3 \right\} - m^3/2^4 \right]. \quad (119)$$

Choosing  $\varepsilon = (m^3/2^4) \left\{ LM + 2^{1/2} L^2 + 2^{-3/2} \bar{\gamma}^{1/2} L^3 \right\}^{-1}$  concludes the proof.  $\square$

**Lemma 17.** *Let  $\bar{\gamma} > 0$  and  $\gamma \in (0, \bar{\gamma}]$ . Then, for any  $x \in \mathbb{R}^d$ ,  $\|x\| \geq 20\sqrt{2\bar{\gamma}d}$ ,*

$$\int_{\mathbb{R}^d \setminus B(0, \|x\|/(4\sqrt{2\bar{\gamma}}))} \varphi(z) dz \leq \exp(-\|x\|^2/(128\gamma)). \quad (120)$$

*Proof.* Let  $x > 0$ . By (Laurent and Massart, 2000, Lemma 1),

$$\mathbb{P}(\|Z\|^2 \geq 2\{\sqrt{d} + \sqrt{x}\}^2) \leq \mathbb{P}(\|Z\|^2 \geq d + 2\sqrt{dx} + 2x) \leq e^{-x}, \quad (121)$$

where  $Z$  is a  $d$ -dimensional standard Gaussian vector. Setting  $t = 2\{\sqrt{d} + \sqrt{x}\}^2$ , we obtain

$$\mathbb{P}(\|Z\|^2 \geq t) \leq \exp\left(-\left\{d + t/2 - \sqrt{2td}\right\}\right), \quad (122)$$

and for  $\sqrt{t} \geq 5\sqrt{d}$ , we get  $\mathbb{P}(\|Z\| \geq \sqrt{t}) \leq e^{-t/4}$  which gives the result.  $\square$

**Proposition 18.** *Assume H1 and H2. Then there exist  $\bar{\gamma} > 0$ ,  $\varpi > 0$ , and  $K_2, \bar{b} \geq 0$  such that for any  $\gamma \in (0, \bar{\gamma}]$  and  $x \in \mathbb{R}^d$ ,*

$$R_{\gamma} V_{\bar{\eta}}(x) \leq (1 - \varpi\gamma) V_{\bar{\eta}}(x) + \bar{b}\gamma 1_{B(0, K_2)}(x), \quad (123)$$

where  $V_{\bar{\eta}}$  is defined by (89),  $R_{\gamma}$  is the MALA kernel given in (80) and  $\bar{\eta}$  is given by (95).

*Proof.* Let  $\bar{\gamma}_1 = m/(4L^2)$ . By Lemma 14, for any  $\gamma \in (0, \bar{\gamma}_1]$  and  $x \in \mathbb{R}^d$ ,

$$R_{\gamma} V_{\bar{\eta}}(x) \leq Q_{\gamma} V_{\bar{\eta}}(x) + V_{\bar{\eta}}(x) \int_{\mathbb{R}^d} \{1 - \min(1, e^{-\tau_{\gamma}^{\text{MALA}}(x, z)})\} \varphi(z) dz \quad (124)$$

$$\leq e^{-\bar{\eta}m\gamma\|x\|^2/4} V_{\bar{\eta}}(x) + b_{\bar{\eta}}\gamma 1_{B(0, K_3)}(x) + V_{\bar{\eta}}(x) \int_{\mathbb{R}^d} \{1 - \min(1, e^{-\tau_{\gamma}^{\text{MALA}}(x, z)})\} \varphi(z) dz, \quad (125)$$

where  $K_3$  and  $b_{\bar{\eta}}$  are given in (95). Let

$$\bar{\gamma}_2 = \min(1, \bar{\gamma}_1, m^3/(4L^4)), \quad M_1 = \max(1, 2K_1, K_2, K_3, 20\sqrt{2\bar{\gamma}_2 d}). \quad (126)$$

Then, by Lemma 16 and Lemma 17, there exist  $C_1 \geq 0$  such that for any  $x \in \mathbb{R}^d$ ,  $\|x\| \geq M_1$  and  $\gamma \in (0, \bar{\gamma}_2]$ ,

$$R_{\gamma} V_{\bar{\eta}}(x) \leq e^{-\bar{\eta}m\gamma\|x\|^2/4} V_{\bar{\eta}}(x) + V_{\bar{\eta}}(x) \{C_1\gamma + \exp(-\|x\|^2/(128\gamma))\} \quad (127)$$

$$\leq e^{-\bar{\eta}m\gamma\|x\|^2/4} V_{\bar{\eta}}(x) + V_{\bar{\eta}}(x) \{C_1\gamma + \exp(-1/(128\gamma))\}. \quad (128)$$

Using that there exists  $C_2 \geq 0$  such that  $\sup_{t \in (0,1)} \{t^{-1} \exp(-1/(128t))\} \leq C_2$  we get for any  $x \in \mathbb{R}^d$ ,  $\|x\| \geq M_1$ ,  $\gamma \in (0, \bar{\gamma}_2]$ ,

$$R_\gamma V_{\bar{\eta}}(x) \leq e^{-\bar{\eta}m\gamma\|x\|^2/4} V_{\bar{\eta}}(x) + V_{\bar{\eta}}(x)\gamma \{C_1 + C_2\} . \quad (129)$$

Let

$$M_2 = \max \left( M_1, 4(C_1 + C_2)^{1/2}(\bar{\eta}m)^{-1/2} \right) , \quad \bar{\gamma}_3 = \min \left( \bar{\gamma}_2, 4 \{m\bar{\eta}M_2^2\}^{-1} \right) . \quad (130)$$

Then, since for any  $t \in [0, 1]$ ,  $e^{-t} \leq 1 - t/2$ , we get for any  $x \in \mathbb{R}^d$ ,  $\|x\| \geq M_2$ ,  $\gamma \in (0, \bar{\gamma}_3]$ ,

$$\begin{aligned} R_\gamma V_{\bar{\eta}}(x) &\leq e^{-\bar{\eta}m\gamma M_2^2/4} V_{\bar{\eta}}(x) + V_{\bar{\eta}}(x)\gamma \{C_1 + C_2\} \\ &\leq [1 - \gamma \{\bar{\eta}mM_2^2/8 - C_1 - C_2\}] V_{\bar{\eta}}(x) \\ &\leq \{1 - \gamma\bar{\eta}mM_2^2/16\} V_{\bar{\eta}}(x) . \end{aligned} \quad (131)$$

In addition, by Equation (110), using that for any  $t \in \mathbb{R}$ ,  $1 - \min(1, e^{-t}) \leq |t|$ , there exists  $C_3 \geq 0$  such that for any  $x \in \mathbb{R}^d$ ,  $\|x\| \leq M_2$  and  $\gamma \in (0, \bar{\gamma}_3]$ ,

$$R_\gamma V_{\bar{\eta}}(x) \leq V_{\bar{\eta}}(x) + b_{\bar{\eta}}\gamma 1_{B(0, K_3)}(x) + C_3\gamma^{3/2} \int_{\mathbb{R}^d} \{1 + \|x\|^2 + \|z\|^4\} \varphi(z) dz \quad (132)$$

$$\leq (1 - \gamma\bar{\eta}mM_2^2/16) V_{\bar{\eta}}(x) + \gamma\bar{\eta}mM_2^2 e^{\bar{\eta}M_2^2/16} + \gamma b_{\bar{\eta}} \quad (133)$$

$$+ C_3\gamma\bar{\gamma}_3^{1/2} \{1 + M_2^2 + C_4\} , \quad (134)$$

where  $C_4 = \int_{\mathbb{R}^d} \|z\|^4 \varphi(z) dz$ . Hence, (123) holds with

$$\varpi = \bar{\eta}mM_2^2/16, \quad \bar{b} = \bar{\eta}mM_2^2 e^{\bar{\eta}M_2^2/16} + b_{\bar{\eta}} + C_3\bar{\gamma}_3^{1/2} \{1 + M_2^2 + C_4\} . \quad (135)$$

□

## E Algorithms

In this section, we have compiled the detailed description of all the algorithms we use in the text:

- Algorithm 4 for i-SIR;
- Algorithm 5 for Ex<sup>2</sup>MCMC with independent proposals;
- Algorithm 6 for Ex<sup>2</sup>MCMC with dependent proposals.

The unifying information for the hyperparameter selection in all the considered experiments is given in Table 6.

---

### Algorithm 4: Single stage of i-SIR algorithm with independent proposals

---

**Input** : Sample  $Y_j$  from previous iteration  
**Output**: New sample  $Y_{j+1}$

- 1 Set  $X_{j+1}^1 = Y_j$  and draw  $X_{j+1}^{2:N} \sim \Lambda$ .
- 2 **for**  $i \in [N]$  **do**
- 3   compute the normalized weights  $\omega_{i,j+1} = \tilde{w}(X_{j+1}^i) / \sum_{k=1}^N \tilde{w}(X_{j+1}^k)$ .
- 4   Set  $I_{j+1} = \text{Cat}(\omega_{1,j+1}, \dots, \omega_{N,j+1})$ .
- 5   Draw  $Y_{j+1} = X_{j+1}^{I_{j+1}}$ .

---

## F Numerical experiments

We provide here additional information to the simulation problems of the main document and present results on new simulation problems.

**Algorithm 5:** Single stage of Ex<sup>2</sup>MCMC algorithm with independent proposals

---

**Input** : Sample  $Y_j$  from previous iteration  
**Output:** New sample  $Y_{j+1}$

- 1 Set  $X_{j+1}^1 = Y_j$  and draw  $X_{j+1}^{2:N} \sim \Lambda$ .
- 2 **for**  $i \in [N]$  **do**
- 3   | compute the normalized weights  $\omega_{i,j+1} = \tilde{w}(X_{j+1}^i) / \sum_{k=1}^N \tilde{w}(X_{j+1}^k)$ .
- 4 Set  $I_{j+1} = \text{Cat}(\omega_{1,j+1}, \dots, \omega_{N,j+1})$ .
- 5 Draw  $Y_{j+1} \sim \mathcal{R}(X_{j+1}^{I_{j+1}}, \cdot)$ .

---

**Algorithm 6:** Proposal generation procedure for FlEx<sup>2</sup>MCMC algorithm with dependent proposal

---

**Input** : Sample  $Y_j$  from previous iteration  
**Output:** Set of proposals for the current iteration  $X_{j+1}^{1:N}$

- 1 Draw  $U_{j+1} \sim \text{Unif}([N])$  and set  $X_{j+1}^{U_{j+1}} = Y_j$
- 2 Set  $Z_{j+1}^{U_{j+1}} = T_{\theta_j}^{-1}(X_{j+1}^{U_{j+1}})$
- 3 Draw  $\alpha_{j+1}^{U_{j+1}} \sim \nu$
- 4 Draw  $\xi_{j+1} \sim N(\alpha_{j+1}^{U_{j+1}} Z_{j+1}^{U_{j+1}}, \sigma_\Lambda^2 (1 - (\alpha_{j+1}^{U_{j+1}})^2) \text{Id})$
- 5 For  $i \in [N] \setminus \{U_{j+1}\}$ , draw  $W_{j+1}^i \sim N(0, \text{Id}_d)$  and  $\alpha_{j+1}^i \sim \nu$  and set  
 $Z_{j+1}^i = \alpha_{j+1}^i \xi_{j+1} + \sqrt{1 - \{\alpha_{j+1}^i\}^2} W_{j+1}^i$ .
- 6 Set  $X_{j+1}^{1:N \setminus \{U_{j+1}\}} = T_{\theta_j}(Z_{j+1}^{1:N \setminus \{U_{j+1}\}})$

---

**Algorithm 7:** Single stage of FlEx<sup>2</sup>MCMC with independent proposals. Steps 1-7 are done in parallel for independent chains indexed by  $k$  but with common values of proposal parameters  $\theta_j$ . Step 9 updates the parameters using the gradient estimate obtained from all the chains.

---

**Input** : weights  $\theta_j$ , batch  $Y_j[1 : K]$   
**Output:** new weights  $\theta_{j+1}$ , batch  $Y_{j+1}[1 : K]$

- 1 **for**  $k \in [K]$  **do**
- 2   | Set  $X_{j+1}^1[k] = Y_j[k]$ .
- 3   | Draw  $Z_{j+1}^{1:N \setminus \{1\}}[k] \sim \Lambda$ .
- 4   | Set  $X_{j+1}^{1:N \setminus \{1\}}[k] = T_{\theta_j}(Z_{j+1}^{1:N \setminus \{1\}}[k])$ .
- 5   | **for**  $i \in [N]$  **do**
- 6   |   | compute the unnormalized weights  $\bar{\omega}_{i,j+1}[k] = \tilde{w}_{\theta_j}(X_{j+1}^i[k])$ .
- 7   |   | Compute  $\Omega_N[j+1, k] = \sum_{i=1}^N \bar{\omega}_{i,j+1}[k]$  and the normalized weights  $\omega_{i,j+1}[k] = \bar{\omega}_{i,j+1}[k] / \Omega_N[j+1, k]$ .
- 8   |   | Set  $I_{j+1}[k] = \text{Cat}(\omega_{1,j+1}[k], \dots, \omega_{N,j+1}[k])$ .
- 9   |   | Draw  $Y_{j+1}[k] \sim \mathcal{R}(X_{j+1}^{I_{j+1}}[k], \cdot)$ .
- 10 | Draw  $\bar{Z}[1 : K] \sim \Lambda$ .
- 11 | Update  $\theta_{j+1} = \theta_j - \gamma \widehat{\nabla \mathcal{L}}(Y_{j+1}, \bar{Z}, \theta_j)$ .

---

## F.1 Metrics

**ESTD** To compute ESTD, we perform 10 random one-dimensional projections and then perform Kernel Density Estimation there for reference and produced samples, and take TV-distance between two distributions over 1D grids of 1000 points. We consider the value averaged over the projections to show the divergence between the MCMC distribution and the reference distribution.

**EEMD** We compute the EEMD as the transport cost between sample and reference points in  $L_2$  using the algorithm proposed in Bonneel et al. (2011).

Experiment	Method	burn-in steps	sampl. steps	$\gamma$	$N$	$\epsilon$	$\alpha$	num MALA steps	num flows	batch size	num train steps	lr
Funnel, Banana	MALA		50k	.01								
	Ex <sup>2</sup> MCMC		1k	.01	10	.5	.9	50				
	FlEx <sup>2</sup> MCMC		1k	.01	10	.5	.9	50	6	200	200	.005
Bayesian Logistic Regression	i-SIR		3k		5							
	MALA		3k	.01								
	Ex <sup>2</sup> MCMC		3k	.01	5	.5	.9	1				
	FlEx <sup>2</sup> MCMC		3k	.01	5	.5	.9	1	4	100	200	.01
Gaussian	i-SIR		15k		10							
	Ex <sup>2</sup> MCMC		15k		10	1.	.95	0				
Mixture of two Gaussian distributions	i-SIR	100	900		10							
	MALA	100	900	.01								
	Ex <sup>2</sup> MCMC	100	900	.01	5	.5	.9	1				
	FlEx <sup>2</sup> MCMC	100	900	.01	5	.5	.9	1	2	100	200	0.01
Mixture of 25 Gaussian distributions	MALA		1k	.001								
	Ex <sup>2</sup> MCMC		1k	.001	10	1.	.9	1				
Mixture of 243 Gaussian distributions	MALA		1.5k	.001								
	Ex <sup>2</sup> MCMC		1.5k	.001	10	.9	.99	1				
Swissroll	MALA		5k	.001								
	Ex <sup>2</sup> MCMC		5k	.001	10	.5	.9	1				
Allen-Cahn equation	(Gabrié et al. (2021))			.001				10	2	100	10k	.001
	Ex <sup>2</sup> MCMC			.001	10	.5	.9	10	2	100	10k	.001
Ill-conditioned Gaussian distribution	MALA			.01								
	Ex <sup>2</sup> MCMC			.01	10							
	FlEx <sup>2</sup> MCMC			.01	10	.5	.9	10	2	100	10k	.001

Table 6: Hyperparameters used in experiments.

**ESS** The ESS is computed as follows: for sample  $\{Y_t\}_{t=1}^M$ ,  $Y_t \in \mathbb{R}^d$  of size  $M$ , we compute ESS component-wise. To be specific, for  $i = 1, \dots, d$ , we compute

$$\text{ESS}_i = \frac{M}{1 + \sum_{k=1}^M \rho_k^{(i)}} ,$$

where  $\rho_k^{(i)} = \frac{\text{Cov}(Y_{t,i}, Y_{t+k,i})}{\text{Var}(Y_{t,i})}$  is the autocorrelation at lag  $k$  for  $i$ -th component. We replace  $\rho_k$  by its sample counterpart. Then we compute

$$\text{ESS} = d^{-1} \sum_{i=1}^d \text{ESS}_i .$$

## F.2 Normalizing flow RealNVP

We use RealNVP architecture (Dinh et al. (2017)) for our experiments with adaptive MCMC. The key item of RealNVP is a coupling layer, defined as transformation  $f : \mathbb{R}^D \rightarrow \mathbb{R}^D$ :

$$y_{1:d} = x_{1:d} \tag{136}$$

$$y_{d+1:D} = x_{d+1:D} \odot \exp(s(x_{1:d}) + t(x_{1:d})) \tag{137}$$

where  $s$  and  $t$  are some functions from  $\mathbb{R}^D$  to  $\mathbb{R}^D$ . It is clear then that the Jacobian of such transformation is triangular matrix with nonzero diagonal terms. We use fully connected neural networks to parameterize the functions  $s$  and  $t$ .

In all experiments with normalizing flows, we use optimizer Adam (Kingma and Ba (2015)) with  $\beta_1 = 0.9$ ,  $\beta_2 = 0.999$  and weight decay 0.01 to avoid overfitting.

## F.3 Adaptive strategy for tuning the stepsize in the MALA algorithm

In all our experiments, except for the Allen-Cahn equation, we use adaptive strategy for the stepsize in MALA, Ex<sup>2</sup>MCMC and FlEx<sup>2</sup>MCMC algorithms to keep acceptance rate close to  $\alpha = 0.5$ : we measure the average acceptance rate  $\mu_{acc}$  during sampling, and increase the stepsize if  $\mu_{acc} > \alpha$  or decrease it if  $\mu_{acc} < \alpha$  with some tolerance threshold. The scheme is described in Algorithm 8. In practice, we set tolerance  $\delta = 0.03$ , factor  $s = 1.05$ .

---

**Algorithm 8:** Adaptive strategy for stepsize.

---

**Input** : average acc. rate  $\mu_{acc}$ , target acc. rate  $\alpha$ , current stepsize  $\gamma$ , tolerance  $\delta$ , factor  $s$   
**Output:** new stepsize  $\gamma'$

```

1 if  $\mu_{acc} - \alpha > \delta$  then
2   |  $\gamma' = \gamma s$ 
3 else if  $\alpha - \mu_{acc} > \delta$  then
4   |  $\gamma' = \gamma / s$ 
5 else
6   |  $\gamma' = \gamma$ 

```

---

Note that in all experiments, wherever it is not said otherwise, we set noise scale coefficient in MALA kernel to  $\sqrt{2\gamma}$ , where  $\gamma$  is step size.

## F.4 High-dimensional Gaussian distribution sampling

We consider the problem of sampling from a high-dimensional standard Normal distribution  $\mathcal{N}(0, \text{Id}_d)$  and the proposal distribution  $\mathcal{N}(0, 2 \text{Id}_d)$  for different problem dimension  $d \in [30; 300]$ . The goal of the experiment is to show the efficiency of correlated proposals for i-SIR. We apply Ex<sup>2</sup>MCMC algorithm with  $\epsilon = 1$  and without rejuvenation kernel, as it is described in Algorithm 6. We compute empirical estimates of mean and variance, and report confidence intervals for them based on 20 independent runs of each algorithm. We report empirical estimates of mean and variance, and the ESS. We perform  $10^3$  burn-in steps for each of the algorithms, and then compute the metrics over the next  $5 \times 10^3$  samples. Other experimental details are provided in Table 6.

## F.5 Distributions with complex geometry

In this section, we study the sampling quality from high-dimensional distributions, whose density levels have high curvature (Banana shaped and Funnel distributions, details below). With such distributions, standard MCMC algorithms like MALA or i-SIR, fail to explore fully the density support. In the examples below, we sample reference points with HMC-type algorithm NUTS (Hoffman et al. (2014)). For each of examples we produce 1000 reference points from the target distribution and consider them as reference points to compute ESTV and EMD for samples from MALA, Ex<sup>2</sup>MCMC and FlEx<sup>2</sup>MCMC. For every target distribution, we set proposal to be the standard normal distribution  $\mathcal{N}(0, \text{Id}_d)$ . As we do 50 rejuvenation steps in Ex<sup>2</sup>MCMC and FlEx<sup>2</sup>MCMC algorithms, we take every 50th point from MALA samples to compute ESS. We set proposal as standard normal distribution for all target distributions.

**Symmetric banana-shaped distribution** Following Haario et al. (1999), we sample from the so-called “Banana-shape” distribution. For  $x \in \mathbb{R}^{2d}$ , the density of the symmetric banana-shaped distribution is given by

$$p(x) = \frac{1}{Z} \exp \left( \sum_{i=1}^d -(x_{2i-1} - x_{2i}^2) / \nu - (x_{2i-1} - 1)^2 \right), \quad (138)$$

with  $Z$  being a normalizing constant and  $\nu > 0$ . In our examples we set  $\nu = 0.2$ .

**Asymmetric banana-shaped distribution** For  $x \in \mathbb{R}^{2d}$ , the density of the asymmetric banana-shaped distribution is given by

$$p(x) = \frac{1}{Z} \exp \left( \sum_{i=1}^d -(x_{2i-1} - x_{2i}^2) / \nu - (x_{2i} - 1)^2 \right), \quad (139)$$

with  $Z$  being a normalizing constant and  $\nu > 0$ . In our examples we set  $\nu = 0.2$ .

**Funnel distribution** For  $x \in \mathbb{R}^{2d}$  the density of the funnel distribution is given by

$$p(x) = \frac{1}{Z} \exp \left( -\frac{x_1^2}{2a^2} - e^{-2bx_1} \sum_{i=2}^{2d} \{x_i^2 - \log d + 2bx_1\} \right), \quad (140)$$

where  $Z$  is a normalizing constant. We set  $a = 1$ ,  $b = 0.5$ .

Results for both types of banana-shaped distributions and for the funnel distribution are summarized in Figure 14 and in Figure 10, respectively. We report the values of ESTV, EEMD, and ESS metrics and their dependence on the problem dimension  $d$ . Clearly, FlEx<sup>2</sup>MCMC algorithm outperforms both MALA and Ex<sup>2</sup>MCMC with independent proposals. We visualize projections of generated samples on first two coordinates for the banana-shaped and funnel examples in Figure 13 and Figure 13c, respectively. They illustrate how well Ex<sup>2</sup>MCMC and FlEx<sup>2</sup>MCMC can explore the support compared to MALA.

## F.6 Bayesian Logistic regression

The training set  $\mathcal{D}$  consists of pairs  $(x, y)$  where  $x = (x^{(0)}, \dots, x^{(d-1)}) \in \mathbb{R}^d$  and labels  $y \in \{-1, 1\}$ . In practice, the first coordinate of  $x$  represents the bias term, i.e. we have  $x^{(0)} = 1$ . The likelihood for a pair is  $p(y | x, \theta) = \text{logit}(y \langle x, \theta \rangle)$ . Given a prior distribution  $p(\theta)$ , we sample from the posterior distribution  $p(\theta | \mathcal{D})$  and compute the predictive posterior  $p(y | x, \mathcal{D}) = \int p(y | x, \theta) p(\theta | \mathcal{D}) d\theta$  for  $(x, y) \in \mathcal{D}^{\text{test}}$ . We approximate  $p(y | x, \mathcal{D})$  using the Monte Carlo estimate  $\frac{1}{n} \sum_{i=1}^n p(y | x, \mathcal{D}, \theta_i)$ , where  $\theta_i$  is a sample of  $p(\theta | \mathcal{D})$  obtained using different MCMC samplers. We take a normal prior distribution  $p_0(\theta) = \mathcal{N}(0, \sigma^2 \text{Id})$  with  $\sigma^2 = 20$ . We present results for the following datasets:

*Covertype* dataset consists of 581k instances of dimension 54, and we arbitrarily classes 3 and 5 from the original 7 classes to build a binary classification task. We used 1.5k steps for burn-in and sampling phases.

*EEG* dataset consists of 15k instances of dimension 15. We used 1.5k steps for burn-in and sampling phases.

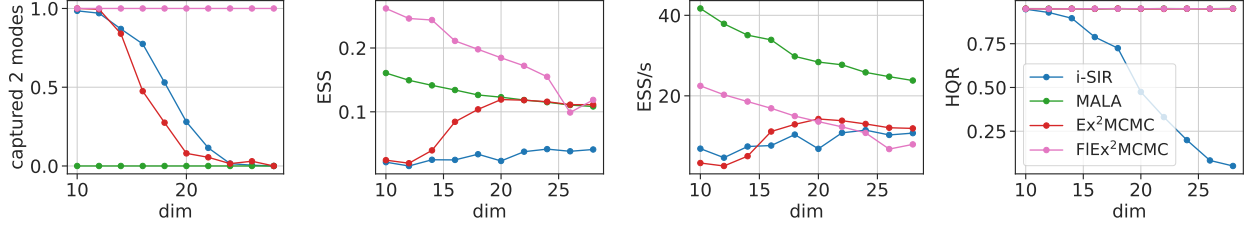


Figure 9: Sampling from mixture of two Gaussian distributions  $\mathcal{N}(-1.5, \text{Id}), \mathcal{N}(1.5, \text{Id})$  in high dimensions.

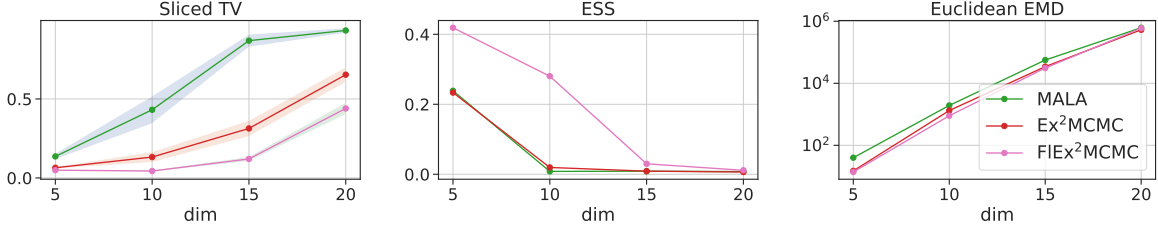


Figure 10: Sampling from Funnel distribution.

*Digits* dataset consists of 1.8k instances of dimension 64, and we kept arbitrarily classes 5 and 6 from the original 10 classes for binary classification task. We used 1.5k steps for burn-in and sampling phases.

We randomly take 0.8 of the dataset for the train set and the rest for the test set. We remove outliers from training set using Isolation Forest classifier.

## F.7 Mixture of two Gaussian distributions

We consider here the task of sampling from a mixture of two Gaussian distributions in different dimensions. The target density is

$$p(x) = \frac{1}{2} g(x; \mu, \sigma^2 \text{Id}_d) + \frac{1}{2} g(x; -\mu, \sigma^2 \text{Id}_d), \text{ where } \mu = (1.5, 1.5, \dots, 1.5) \in \mathbb{R}^d, \sigma^2 = 1,$$

and we set the proposal distribution to be  $\mathcal{N}(0, 2 \text{Id}_d)$ . We perform 200 independent starts for each method for each dimension in  $[10, 12, \dots, 30]$  to compute metrics and average them across different starts. We put more details on hyperparameters used in table 6. We compute ESS per second (ESS/s) as a product of ESS and size of obtained sample (900) divided by sampling time in seconds. The result of this experiment is presented in Figure 9. Note that, despite the ESS of MALA is good, MALA always explores only one mode of the mixture.

## F.8 Allen-Cahn equation

In this experiment, we consider the task of sampling from the invariant distribution of the Allen-Cahn stochastic differential equation (Allen and Cahn (1975)). We borrow the setting from the paper Gabrié et al. (2021) in which they propose to use normalizing flows to enhance MCMC sampling from distributions with meta-stable states. Allen-Cahn equation is a SDE defined in terms of a random field  $\varphi : [0, 1] \rightarrow \mathbb{R}$  that satisfies

$$\partial_t \varphi = a \partial_s^2 \varphi + a^{-1} (\varphi - \varphi^3) + \sqrt{2\beta^{-1}} \eta(t, s), \quad (141)$$

where  $a > 0$ ,  $\beta$  are parameters,  $s \in [0, 1]$ ,  $\eta$  is a spatio-temporal white noise. Following Gabrié et al. (2021), we impose boundary conditions on  $\varphi : \varphi(s=0) = \varphi(s=1) = 0$ . The invariant measure of the stochastic Allen-Cahn equation is the Gibbs measure associated with the Hamiltonian

$$U(\varphi) = \beta \int_0^1 \left[ \frac{a}{2} (\partial_s \varphi)^2 + \frac{1}{4a} (1 - \varphi(s)^2)^2 \right] ds. \quad (142)$$

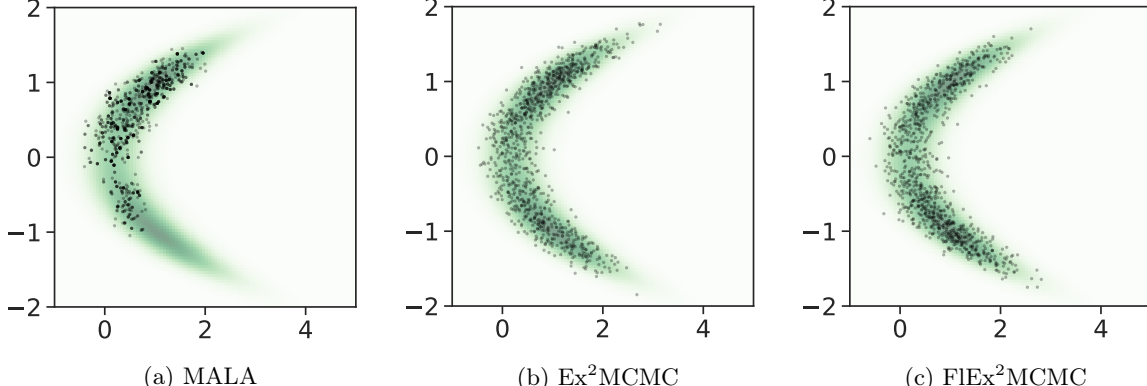


Figure 11: Symmetric banana-shaped distribution, dimension  $d = 50$ : projection of resulted samples on first two coordinates.

The Hamiltonian has two global well separated minima  $\varphi^+$  and  $\varphi^-$ , making it very challenging to sample from the invariant distribution using MCMC methods. Therefore authors propose to use informed base measure with the following Hamiltonian as a proposal

$$U_B(\varphi) = \beta \int_0^1 \left[ \frac{a}{2} (\partial_s \varphi)^2 + \frac{1}{2a} \varphi^2 \right] ds. \quad (143)$$

To perform sampling, we discretize the field on a uniform grid taking 100 points of spatial variable  $s$ . Therefore the dimension of space we sample on is 100.

We set  $a = 0.1$ ,  $\beta = 20$ . We use RealNVP with 2 flows and hidden layer size 50. Other details are provided in the Table 6.

## F.9 Sampling from Ill-Conditioned Gaussian distribution

In this experiment, we consider the task of sampling from zero-centered Gaussian distribution with ill-conditioned covariance being a diagonal matrix with elements spaced log-linearly between  $10^{-2}$  and  $10^2$ . We set the dimension to 50. Figure 12 shows autocorrelation time versus sampling iterations. We perform 50 independent runs of each method to compute autocorrelations and average accross different chains. The experimental details are provided in the Table 6.

## F.10 Sampling from GAN as an Energy-Based Model

In our experiments, we closely follow the exposition of (Che et al., 2020, Section 5), albeit we were not able to exactly reproduce the numbers reported in this paper. We consider the task of sampling in the latent space of learnt GAN model, as presented in Che et al. (2020). The crux of the approach is that under some assumptions on the discriminator being close to the optimal one (given by Bayes rule, see Che et al. (2020)), sampling in latent space from the distribution  $p(z) = \frac{p_0(z)}{Z} \exp(\text{logit}(D(G(z))))$  is equivalent to sampling from the data distribution, where  $p_0(z)$  is a proposal distribution for Generator,  $G$  is a Generator and  $\text{logit}$  is the inverse sigmoid function.

## F.11 GANs as energy-based models: artificial datasets

We tackle in this section the task of sampling artificial datasets. We set the proposal distribution to the standard normal distribution for all datasets.

We pay particular attention to mixture of Gaussian distributions and Swissroll examples. Similar setup is considered at (Azadi et al., 2018; Turner et al., 2019; Tanaka, 2019). We follow the same experimental setting as provided at Tanaka (2019) and (Che et al., 2020, Section 5.1). The main difference compared to (Tanaka, 2019) is that the prior distribution  $p_0$  is a multivariate Gaussian (instead of a uniform).

Table 7: GAN sampling from mixture of Gaussian distributions

Model	Single chain, 25G			Multiple chains, 25G			Single chain, 243G			Multiple chains, 243G		
	std	# modes	EMD	std	# modes	EMD	std	# modes	EMD	std	# modes	EMD
Goodfellow et al. (2014)	.058	25	.064	.058	25	.064	.040	34.8	3.86	.040	34.8	3.86
Che et al. (2020)	.036	1	6.97	.043	25	.062	.022	1	30.96	.039	98	4.20
MALA	.050	25	.2	.058	25	.058	.030	3.5	24.03	.040	85.8	3.80
Ex <sup>2</sup> MCMC	.055	25	.18	.056	25	.18	.030	62.9	3.78	.039	89.4	3.60

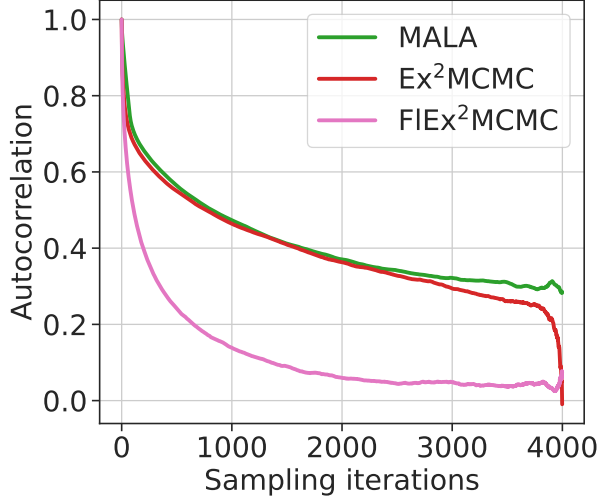


Figure 12: Ill-conditioned Gaussian: Autocorrelations vs. sampling iteration.

**Mixture of 25 Gaussian distributions** We build a dataset of points sampled from a mixture of 25 Gaussian distributions in dimension 2, as in Turner et al. (2019). All Gaussian distributions have scale parameter  $\sigma = 0.05$ , and the coordinates of the means of the Gaussian distributions  $\{\mu_i\}_{i=1}^{25}$  are distributed on a uniform grid:  $\mu_i \in \{-2, -1, 0, 1, 2\}^2$ . From this dataset, we train a WGAN (Arjovsky et al. (2017)). We use 4-layer MLP architectures with hidden dimension 128 and 256 for Generator and Discriminator respectively. We set the dimension of the latent space to  $d = 2$ . We perform 50 independent runs for each method and average metrics across runs. The other experimental details are presented in the Table 6.

**Mixture of 243 Gaussian distributions** To train GAN we construct a dataset from points distributed according to a mixture of 243 Gaussian distributions in dimension 5. All Gaussian distributions have scale parameter  $\sigma = 0.05$ , and the means of the Gaussian distributions  $\{\mu_i\}_{i=1}^{243}$  are distributed on a uniform grid:  $\mu_i \in \{-2, 0, 2\}^5$ . We set the dimension of the latent space to  $d = 5$ . We perform 50 independent runs for each method and average metrics across runs. We use 3-layer MLP architectures for both Generator and Discriminator with hidden dimension 256 and 512 respectively.

**Swissroll** Swissroll is a popular dataset of points in  $2d$  distributed along the spiral with some noise. We set the scale factor of noise  $\sigma = 0.05$ . We set the dimension of the latent space to  $d = 2$ . To train WGAN we use 3-layer MLP architectures for both Generator and Discriminator with hidden dimension 128 and 256 respectively.

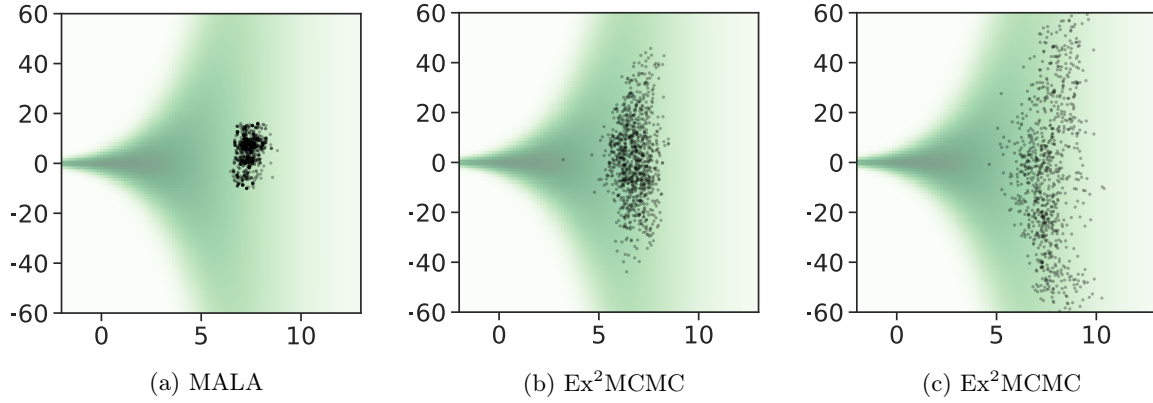


Figure 13: Funnel distribution, dim 15: projection of resulted samples on first two coordinates.

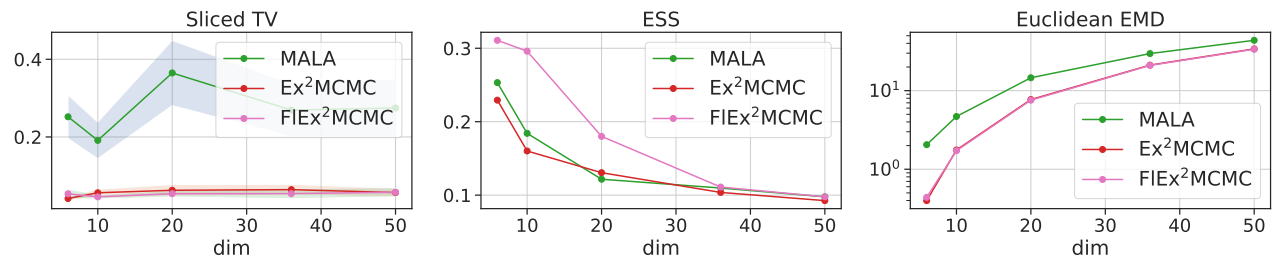


Figure 14: Sampling from symmetric banana-shaped distribution.